Article

SOURCE DATA | TRANSPARENT PROCESS | OPEN ACCESS

EMBO reports

LTK and ALK promote neuronal polarity and cortical migration by inhibiting IGF1R activity

Tania Christova†, Stephanie KY Ho†, Ying Liu, Mandeep Gill & Liliana Attisano*

Abstract

The establishment of axon-dendrite polarity is fundamental for radial migration of neurons, cortical patterning, and formation of neuronal circuits. Here, we show that the receptor tyrosine kinases, Ltk and Alk, are required for proper neuronal polarization. In isolated primary mouse embryonic neurons, the loss of Ltk and/or Alk causes a multiple axon phenotype. In mouse embryos and newborn pups, the absence of Ltk and Alk delays neuronal migration and subsequent cortical patterning. In adult cortices, neurons with aberrant neuronal projections are evident and axon tracts in the corpus callosum are disrupted. Mechanistically, we show that the loss of Alk and Ltk increases the cell-surface expression and activity of the insulin-like growth factor 1 receptor (Igf-1r), which activates downstream PI3 kinase signaling to drive the excess axon phenotype. Our data reveal Ltk and Alk as new regulators of neuronal polarity and migration whose disruption results in behavioral abnormalities.

Keywords ALK; cortical migration; IGF-1R; LTK; neuronal polarity
Subject Category Neuroscience
DOI 10.15252/embr.202356937 | Received 3 February 2023 | Revised 20 April 2023 | Accepted 16 May 2023 | Published online 9 June 2023
EMBO Reports (2023) 24: e56937

Introduction

Neuronal polarization, namely the specification of axon and dendrites, is critical for the development and proper functioning of the brain (Arimura & Kaibuchi, 2007; Barnes & Polleux, 2009; Takano *et al*, 2015). During the early development of the CNS, neural progenitors located in the ventricular zone transition from a multipolar to bipolar state, which enables subsequent radial migration and formation of defined layers that make up the cortex (Noctor *et al*, 2001). In adults, the proper neuronal morphology is critical for signal transmission and for the formation of neuronal circuitry that drives memory, behavior, and all key brain activities (Arimura & Kaibuchi, 2007; Takano *et al*, 2015). In line with this, alterations in neurogenesis, neuronal migration, or morphology can result in neurodevelopmental defects that lead to a variety of neurological and neuropsychiatric disorders (Romero *et al*, 2018). A wide variety of signaling pathways and factors have been identified as regulators of neuronal polarization including Rho GTPases, phosphatidylinositol 3-kinase (PI3K), MAPK pathway components, Wnts and Receptor Tyrosine Kinases (RTKs; Arimura & Kaibuchi, 2007; Lewis Jr. *et al*, 2013; Takano *et al*, 2015).

Leukocyte tyrosine kinase (LTK) and Anaplastic lymphoma kinase (ALK) are closely related Receptor Tyrosine Kinases (RTKs) belonging to the insulin receptor superfamily (Palmer *et al*, 2009; Weiss *et al*, 2012; Roskoski Jr., 2013). ALK was initially described as oncogenic fusion protein in anaplastic large cell lymphomas (ALCL; Shiota *et al*, 1994; Morris *et al*, 1995) and since then, aberrantly activated ALK arising from protein fusions, point mutations or overexpression have been described in many cancers including neuroblastoma (Palmer *et al*, 2009; Hallberg & Palmer, 2016; Janoueix-Lerosey *et al*, 2018). In general, inappropriate engagement of characteristic RTK downstream effectors is thought to mediate the pro-oncogenic activities of these fusion and/or mutant forms of ALK (Palmer *et al*, 2009; Hallberg & Palmer, 2016). Although less studied, LTK dysregulation also has consequences for cancer progression (Muller-Tidow *et al*, 2004; Izumi *et al*, 2021). Accordingly, effective small molecule inhibitors of ALK/LTK have been developed for clinical use, primarily for non-small-cell lung cancers (Awad & Shaw, 2014; Chuang & Neal, 2015). Metastasis to the brain is frequently observed in patients with ALK mutations, an observation that prompted the development of second-round therapeutics, such as lorlatinib, that have successfully addressed the inadequate central nervous system penetration of the first-round inhibitor, crizotinib (Awad & Shaw, 2014; Chuang & Neal, 2015). Ongoing clinical trials have confirmed intracranial activity; however, some changes in cognitive function, mood, and speech in lorlatinib-treated patients have been reported (Solomon *et al*, 2018).

Outside of oncogenic contexts, both ALK and LTK are predominantly expressed in the central and peripheral nervous systems (Iwahara *et al*, 1997; Weiss *et al*, 2012; Janoueix-Lerosey *et al*, 2018). However, in marked contrast to the extensive literature on ALKs in cancer, the normal role of the receptors is much less understood. ALK and/or LTK have been shown to play a role in the development and function of the nervous system. In Zebrafish, LTK promotes the survival and migration of neural crest cells and is required for the specification of the neural crest-derived pigment

Department of Biochemistry, Donnelly Centre, University of Toronto, Toronto, ON, Canada
*Corresponding author. Tel: 416 946-3129; E-mail: liliana.attisano@utoronto.ca
†These authors contributed equally to this work

© 2023 The Authors. Published under the terms of the CC BY NC ND 4.0 license.

cells, called iridophores (Lopes *et al*, 2008; Fadeev *et al*, 2018) while ALK is required for proper neuronal differentiation and survival in the CNS (Yao *et al*, 2013). In *Drosophila*, ALK is required for neuronal circuit assembly in the developing retina and neuromuscular junction, in sparing nervous system growth during nutrient deprivation in larva (Cheng *et al*, 2011), and in adult learning (Gouzi *et al*, 2011). In mice, the overexpression of an activated Alk receptor during embryogenesis results in a disruption of the differentiation of neural crest progenitors (Vivancos Stalin *et al*, 2019), and in an Alzheimer's model of tau proteinopathy, the aberrant activation of Alk leads to the abnormal accumulation and aggregation of phosphorylated Tau and modulates mouse behavior (Park *et al*, 2021). Mice deficient in Alk and/or Ltk are viable and lack gross morphological alterations but do display several subtle behavioral abnormalities, responses to ethanol (Bilsland *et al*, 2008; Lasek *et al*, 2011; Weiss *et al*, 2012), hypogonadotropic hypogonadism in male mice (Witek *et al*, 2015) and resistance to diet-induced obesity (Orthofer *et al*, 2020).

The ligands for LTK and ALK, named ALKAL1 and ALKAL2 (previously referred to as FAM150A/B or Augmentor β/α), were identified relatively recently (Zhang *et al*, 2014; Guan *et al*, 2015; Reshetnyak *et al*, 2015), and a series of recent studies have provided important structural insights into how the ligands engage and activate the receptors via a unique mechanism requiring interactions with the cell membrane (De Munck *et al*, 2021; Li *et al*, 2021; Reshetnyak *et al*, 2021). The ligands have also been shown to be important in CNS development and cancer, acting to specify iridophores in Zebrafish (Mo *et al*, 2017), functioning in the hypothalamus to control body weight in mice (Ahmed *et al*, 2022), mediating persistent pain (Defaye *et al*, 2022) and in driving tumorigenesis in MYCN-driven nonmutant ALK neuroblastomas (Borenas *et al*, 2021) and in a subtype of colon cancer (Mazzeschi *et al*, 2022).

In this study, we sought to understand the physiological role of LTK and ALK in the central nervous system, specifically during cortical development using mouse models. We observed that in the absence of Ltk and Alk, neural progenitor populations, neuronal migration, and subsequent patterning of the cortical layers are disrupted in developing mice and that isolated primary embryonic cortical neurons displayed a multiple axon phenotype. We next investigated the underlying mechanism for the aberrant neuronal phenotype and demonstrate that the loss of Alk and Ltk increases the cell-surface expression and activity of insulin-like growth factor 1 receptors (Igf-1r) that in turn activate downstream PI3 kinase signaling to drive the multiple axon phenotype. Taken together, our data reveal LTK/ALK as new regulators of neuronal morphology and migration. This study thus suggests that it will be important to consider the potential impact on CNS and brain functions in cancer patients being treated with pharmacological inhibitors of ALK/LTK activity.

Results

Ltk and Alk are expressed in the embryonic and adult cortex

ALK and LTK have been extensively studied in cancer, but little is known about the normal biological role of these receptors. Thus, to gain insights into the normal function of Ltk and Alk, we first examined the localized expression of these receptors using single-molecule *in situ* mRNA analysis in the developing cortex. At E15.5, Ltk showed broad expression in the superficial layers (i.e., cortical plate: CP and subcortical plate: SCP) and in intermediate and ventricular/subventricular zones (VZ/SVZ; Fig EV1A and B). Alk expression was also broadly localized, but the highest expression was observed in the proliferating VZ that was marked by Sox2 (Fig EV1A and B). Both receptors were also expressed in several regions outside the neocortex (Fig EV1C–F) consistent with previous findings (Weiss *et al*, 2012; Janoueix-Lerosey *et al*, 2018). Analysis of expression by real-time PCR revealed that both receptors were expressed at E15.5 in the cortex and brain but in differing temporal patterns, with Alk expression maximal at E15.5 and then declining to adulthood, whereas Ltk showed a dramatic enhancement in adults, particularly within the cortex (Fig EV1G).

ALKAL1 and ALKAL2 (also known as FAM150A/Augmentor β and FAM150B/Augmentor α, respectively) are the ligands for LTK and ALK (Zhang *et al*, 2014; Guan *et al*, 2015; Reshetnyak *et al*, 2015). Single-molecule *in situ* hybridization confirmed that Alkal2 was widely expressed in the E15.5 cortex in regions overlapping the Ltk and Alk expression domains including the cortical plate (CP) and ventricular zone (Fig EV1A–F). Analysis by real-time PCR revealed that Alkal2 was expressed in the mouse embryonic, postnatal, and adult cortex and brain at roughly equivalent levels (Fig EV1G). By contrast, Alkal1 expression has not been detected in the mouse brain (Ahmed *et al*, 2022) and according to the Protein Atlas database available at proteinatlas.org (Uhlen *et al*, 2015) Altogether these data show that Alk and Ltk and their ligand, Alkal2 are expressed throughout the embryonic and adult cortex.

Loss of Ltk and Alk disrupts neuronal cell migration and cortical layer patterning in the developing cerebral cortex

To investigate the role of Ltk and Alk in normal physiology, we generated double knockout (*DKO*) mice constitutively lacking both Ltk and Alk ($Ltk^{-/-}Alk^{-/-}$) by crossing homozygous $Ltk^{-/-}$ and $Alk^{-/-}$ single knockout animals. *Ltk* and *Alk* single and *DKO* mice were viable and fertile as previously reported (Bilsland *et al*, 2008; Weiss *et al*, 2012). To investigate the consequences of the loss of Ltk/Alk in the cortex, we first examined the status of progenitor cells in the neurogenic niche. During early cortical development, neural stem cells (NSCs) proliferate symmetrically in the VZ while at the onset of neurogenesis, apical radial glial progenitor (aRG) cells in the VZ divide asymmetrically to produce intermediate neuronal progenitor (INP) cells and postmitotic neurons, both of which lack Sox2 expression (Gotz & Huttner, 2005). Thus, we examined the effect of the loss of *Ltk* and/or *Alk* on progenitor cell populations in E15.5 mice. WT mice displayed the characteristic pattern of Pax6/Sox2-positive aRG cells in the VZ and Tbr2+ INP in the SVZ (Figs 1A and EV2A). However, in single and DKO mice, while the total number of cells ($DAPI^+$) and the number of $Pax6^+$ cells were similar to WT, a marked reduction in both $Sox2^+$ cells, which mark multipotent progenitors and $Tbr2^+$ cells, which indicate INPs, was observed with DKO mice displaying the most dramatic reduction (Figs 1A and EV2B). Thus, the loss of Ltk/Alk results in a disruption of neurogenesis.

Newly born neurons migrate through the intermediate zone (IZ) and give rise to five cortical layers distinguished by the expression

 © 2023 The Authors

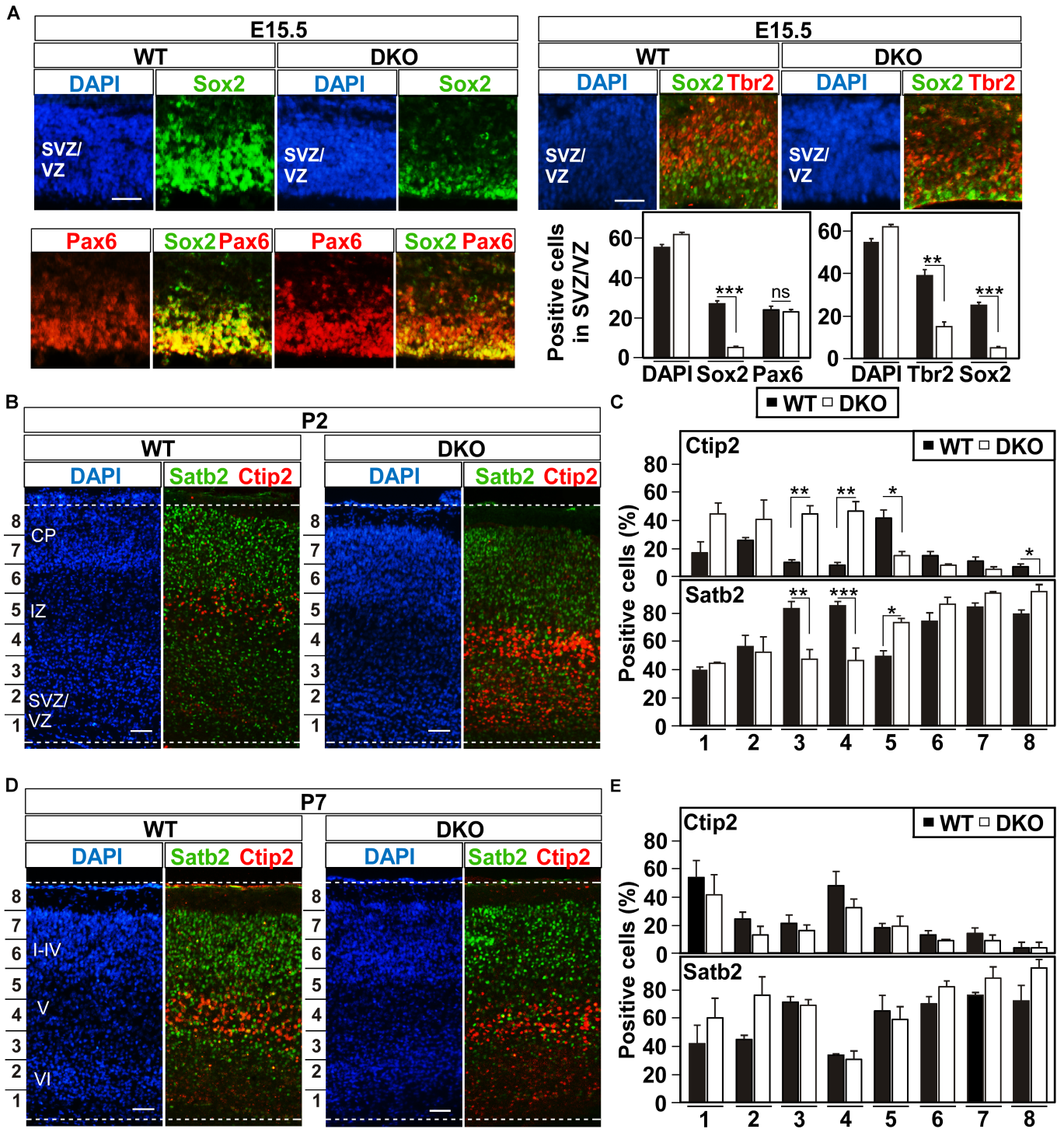


Figure 1. Disruption of Ltk and Alk alters early cortical plate patterning.

A–E (A) Coronal section of E15.5 wild-type (WT) and DKO developing cortices were co-stained with either anti-Sox2 (green) and anti-Pax6 (red) or with anti-Sox2 (green) and anti-Tbr2 (red) and both counterstained with DAPI (blue). Scale bars are 50 μm. Quantitation of total DAPI$^+$ cells and Sox2$^+$, Pax6$^+$, or Tbr2$^+$ progenitor cells in the SVZ/VZ in the entire image, corresponding to an area of 100 × 100 μM are plotted. (B, D) Coronal sections of WT and DKO developing cortices stained with DAPI (blue) and co-stained with anti-Ctip2 (red) and Satb2 (green) at P2 and P7. The location of the cortical plate (CP), intermediate zone (IZ), subventricular/ventricular zone (SVZ/VZ) in P2 mice, and Layers I-VI in P7 WT mice are indicated. Scale bars are 50 μm. (C, E) Quantitation of Ctip2$^+$ and Satb2$^+$ progenitor cells as a percent of total DAPI$^+$ cells in each of 8 bins (marked on left) within the cortex (dashed lines) from a total area corresponding to 100 × 600 μM are plotted.

Data information: Data in (A, C and E) are presented as mean ± SEM of three independent biological experiments. Statistical significance: ***P < 0.001, **P < 0.01, *P < 0.05, Student's t-test.

© 2023 The Authors

of distinct transcription factors that control cortical neuronal identities and properties (Molyneaux *et al*, 2007; Uzquiano *et al*, 2018). Thus, to investigate whether postmitotic regions of the developing cortex were also affected by the loss of Ltk and Alk, we next examined the localization of two layer-specific markers, Ctip2, and Satb2 in WT and knockout mice. At postnatal day 2 (P2), a timepoint in which neurogenesis and migration have primarily subsided, WT Ctip2$^+$ cells are primarily localized to the IZ (bins 5/6) in WT mice, while in DKO mice, the percent of Ctip2$^+$ cells in this region was notably reduced with many Ctip2-positive cells also localized to the lower layers (bins 1–4, marked SVZ/VZ in WT mice: Fig 1B and C). By P7, when neuronal migration is largely completed, the localization of Ctip2$^+$ neurons in DKOs was more similar to the WT, though some Ctip2-positive cells were still observed in the lowest layers (i.e., bins 1–4, labeled Layer VI in WT mice; Fig 1D and E). In the case of Satb2, a reduction in the percent of positive cells in some of the lower layers was observed in mutants at P2 (bins 3 and 4), possibly due to the high proportion of Ctip2$^+$ cells in this region, which was resolved by P7 (Fig 1B–E). The improvement was also evident in Nissl-stained sections of adults where DKO cortices did not display any cytoarchitectural defects (Appendix Fig S1A). Analysis of single *Ltk*$^{-/-}$and *Alk*$^{-/-}$ mice at P2 and P7 revealed similar, though more modest disruptions in the localization of Ctip2- and Satb2-positive neurons (Fig EV2C–F). The overall number of Ctip2- and Satb2-positive neurons was similar in all genotypes (Appendix Fig S2). Thus, given that Ctip2-positive neurons were present in similar numbers but showed altered timing of proper localization, our observations suggest that the loss of *Ltk* and *Alk* results in a delay in migration rather than in a disruption in neuronal subtype specification.

We next sought further evidence that the alterations in patterning of the cortical layers in the absence of Ltk/Alk were due to a disruption in the migration of nascent neurons. For this, embryos were injected with BrdU at E14.5 and were then fixed and stained at E17.5, P2, and P7 (Fig 2). Quantitative analysis revealed that in E17.5 wild-type mice, the majority of BrdU-positive neurons had migrated towards the superficial layers, spanning the entire cortex. By contrast, in single *Ltk*$^{-/-}$ or *Alk*$^{-/-}$ and in *DKO* mice, there was a marked decrease in BrdU-positive neurons reaching the middle and superficial layers (bins 5–8: Fig 2A and B). In P2 WT brains, most of the BrdU-positive neurons were found in bin 6–8 (i.e., the CP), whereas in the *DKOs*, most of the BrdU-positive neurons were scattered throughout the cortex. By P7, the majority of BrdU-positive neurons were found in the superficial layers in both DKO and WT brains (Fig 2C and D). This apparent delay in migration recapitulates the delayed patterning observed using layer-specific markers, Ctip2 and Satb2 shown in Fig 1B–E. Taken together these studies demonstrate a role for Alk/Ltk in promoting neuronal migration during patterning of the developing cortex.

Ltk/Alk regulates neuronal polarity in cortical neurons

Proper neuronal polarization is essential for the migration of nascent neurons (Arimura & Kaibuchi, 2007). Thus, to explore a potential role for Ltk/Alk in neuronal polarization, we turned to freshly isolated and plated primary embryonic cortical neurons, a model system that recapitulates the *in vivo* acquisition of neuronal polarity (Fig 3A) in which a single axon emerges from multiple indistinguishable neurites (Bradke & Dotti, 2000; Barnes & Polleux, 2009). We confirmed by single-molecule RNA *in situ* that the majority (70%) of isolated neurons expressed both Ltk and Alk, roughly 20% expressed only one receptor and about 10% expressed neither (Appendix Fig S3A). We observed that primary cortical neurons isolated from single *Ltk*$^{-/-}$ or *Alk*$^{-/-}$ mice displayed a marked increase in the number of axons, visualized by staining with axonal marker Tau-1 that were negative for the dendritic marker, MAP2, indicating axonal identity (Fig 3B). The simultaneous loss of both Ltk and Alk (i.e., *DKO* neurons) did not further enhance the multiple axon phenotype, suggesting that these receptors do not act redundantly in this context but rather may both be required for proper neuronal polarization function. Conversely, the overexpression of HA-tagged LTK (LTK-WT-HA) inhibited axon formation in wild-type neurons, while in *DKO* neurons, ectopic expression of LTK not only reversed the aberrant multiple axon phenotype but also restored the wild-type single axon morphology (Fig 3C and Appendix Fig S3B). We confirmed these observations by testing the effect of abrogating the expression of *Ltk*, *Alk*, or both in wild-type neurons using siRNAs. Similar to neurons isolated from knockout mice, we observed a marked increase in the number of axons upon loss of Ltk, Alk, or both (Appendix Fig S3C and D) indicating that the effect observed in neurons from KO mice was not due to the emergence of indirect, long-term compensatory mechanisms. As an alternative to genetic approaches, we also treated wild-type embryonic cortical neurons with two small molecules, TAE684, a potent and highly specific inhibitor of ALK (Galetta *et al*, 2012), and crizotinib, a drug in clinical trials for the treatment of ALK fusion protein-positive cancers (Rodig & Shapiro, 2010), which also inhibits LTK (Centonze *et al*, 2019). Neurons treated with either TAE684 or crizotinib also displayed the multiple axon phenotype (Fig 3D). Taken together, these results show that both LTK and ALK are important for proper neuronal polarization in murine cortical neurons and that either abrogation of expression or chemical inhibition of their activities induces the formation of multiple axons.

Ltk and *Alk* knockout mice display defects in neuronal morphology and axon tracts

To investigate whether mice lacking Ltk/Alk display any morphological changes *in vivo*, we visualized neurons in the adult brain using Golgi staining, an approach that enables the visualization of individual neurons. The gross overall morphology of wild-type, single, or double knockout cortices was similar (Fig 3E and Appendix Fig S1B). In wild-type cortices, analysis of layer IV/V revealed that individual pyramidal neurons were fully developed with elaborated dendritic trees, including dendrites with numerous spines and an apparent single axon (distinguished by an absence of spines) extending to the superficial layers of the mature cortex (Fig 3E and Appendix Fig S1B). By contrast, pyramidal neurons in single and double knockout mice exhibited an abnormal pattern of neurites that included aberrant horizontal projections across the cortical layers (red arrows) that were more prominent in *DKO*s. Of note, within the corpus callosum (CC), abnormalities in the axon tracts were observed in both single and double knockout mice (Fig 3F). Thus, although adult mice display an overall normal cortical layering morphology, the loss of either Ltk alone, Alk alone, or both

 © 2023 The Authors

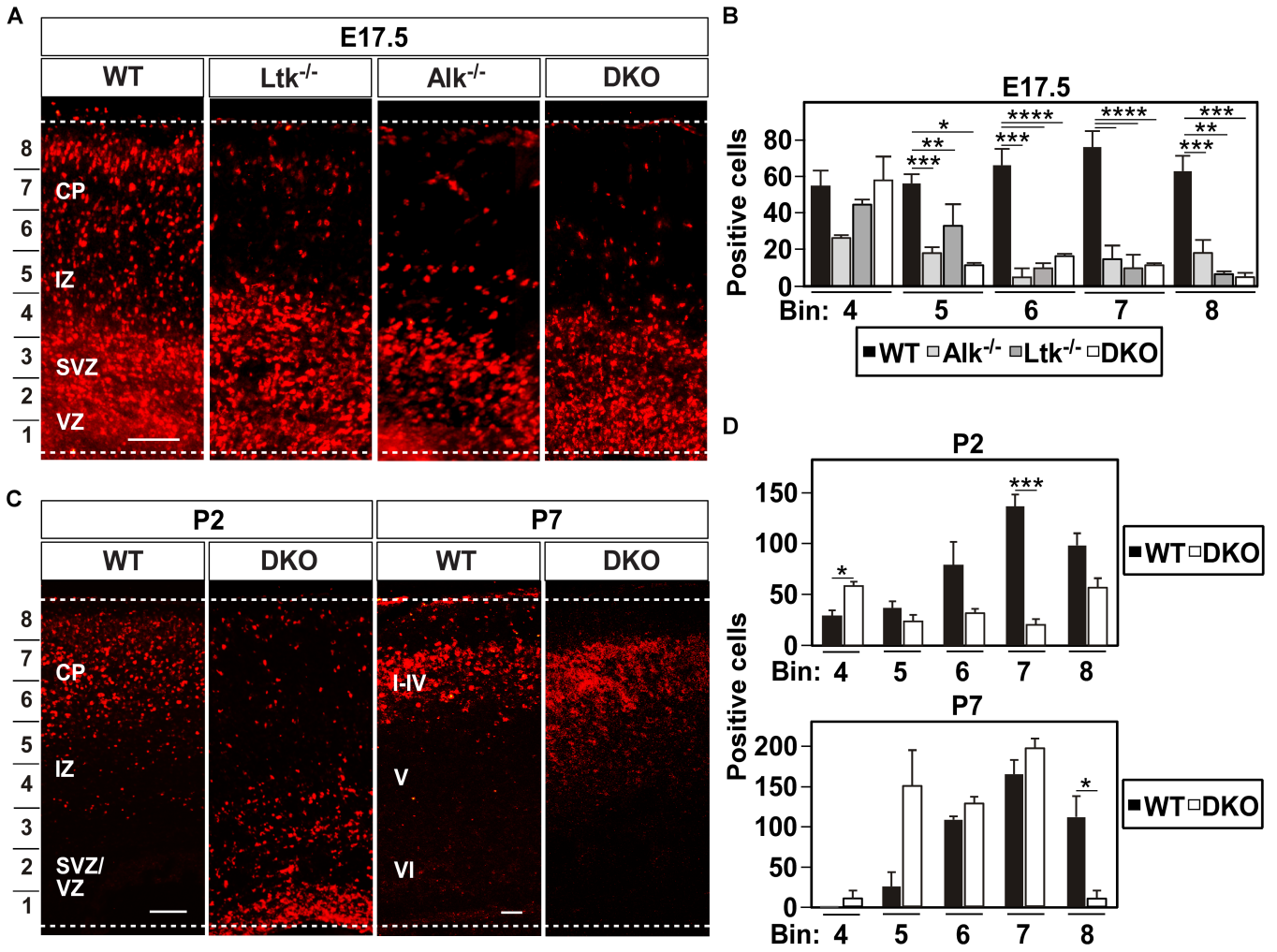


Figure 2. Loss of Ltk/Alk leads to delayed radial migration.

A–D Wild-type (WT), single ($Ltk^{-/-}$ and $Alk^{-/-}$), and double (DKO) knockout embryos were injected with BrdU on day E14.5 and fixed cortices analyzed at E17.5, P2, and P7. (A–C) Coronal sections of BrdU-labeled WT and mutant cortices at the indicated ages. Dotted lines mark the upper and lower cortical limits determined for each section. The location of the cortical plate (CP), intermediate zone (IZ), subventricular/ventricular zone (SVZ/VZ) in E17.5 and P2 mice and Layers I–VI in P7 WT mice are indicated. Scale bars are 50 μm. (B, D) Quantitation in E17.5 (B) or P2 and P7 (D) cortices of BrdU-positive cells in the indicated bins (marked on left of images) is plotted.

Data information: Data are presented as the mean ± SEM from 3 (DKO, $Ltk^{-/-}$) or 2 (WT, $Alk^{-/-}$) independent biological experiments (B) or 3 (DKO and WT) independent biological experiments (D). Statistical significance: ****$P < 0.0001$, ***$P < 0.001$, **$P < 0.005$, *$P < 0.05$ by the Student's t-test.
Source data are available online for this figure.

disrupts the morphology of individual neurons and the proper establishment of axon tracts.

Increased anxiety and impaired problem-solving behavior in *DKO* mice

Defects in axons and axon tracts caused by Ltk/Alk deficiency may impact neuronal connectivity and function. Thus, we undertook a series of tests to explore whether these mice display any behavioral abnormalities related to neurodevelopmental disorders, such as deficits in cognitive function and anxiety. We first performed the light–dark test, which is based on the innate aversion of rodents to brightly illuminated areas and on their spontaneous exploratory behavior in response to mild stressors (Bourin & Hascoet, 2003). Mice were placed in an open chamber with bright light and the time to discover the adjacent enclosed dark chamber, as well as the frequency of exit and re-entry into the dark was determined. Analysis of the results showed that the behavior of single $Ltk^{-/-}$ or $Alk^{-/-}$ mutants was similar to that of WT mice at all ages tested (Fig 4A). In the case of *DKO*s, mice displayed higher latency times for entry into the dark area and a significant reduction in transitions (Fig 4A and Appendix Fig S4A), indicative of reduced exploratory behavior and increased anxiety that also became more pronounced with age.

We next employed the Y-maze test for spontaneous alternations, which measures the tendency to make free choices in an alternating manner in the maze and is a paradigm for studying working

© 2023 The Authors

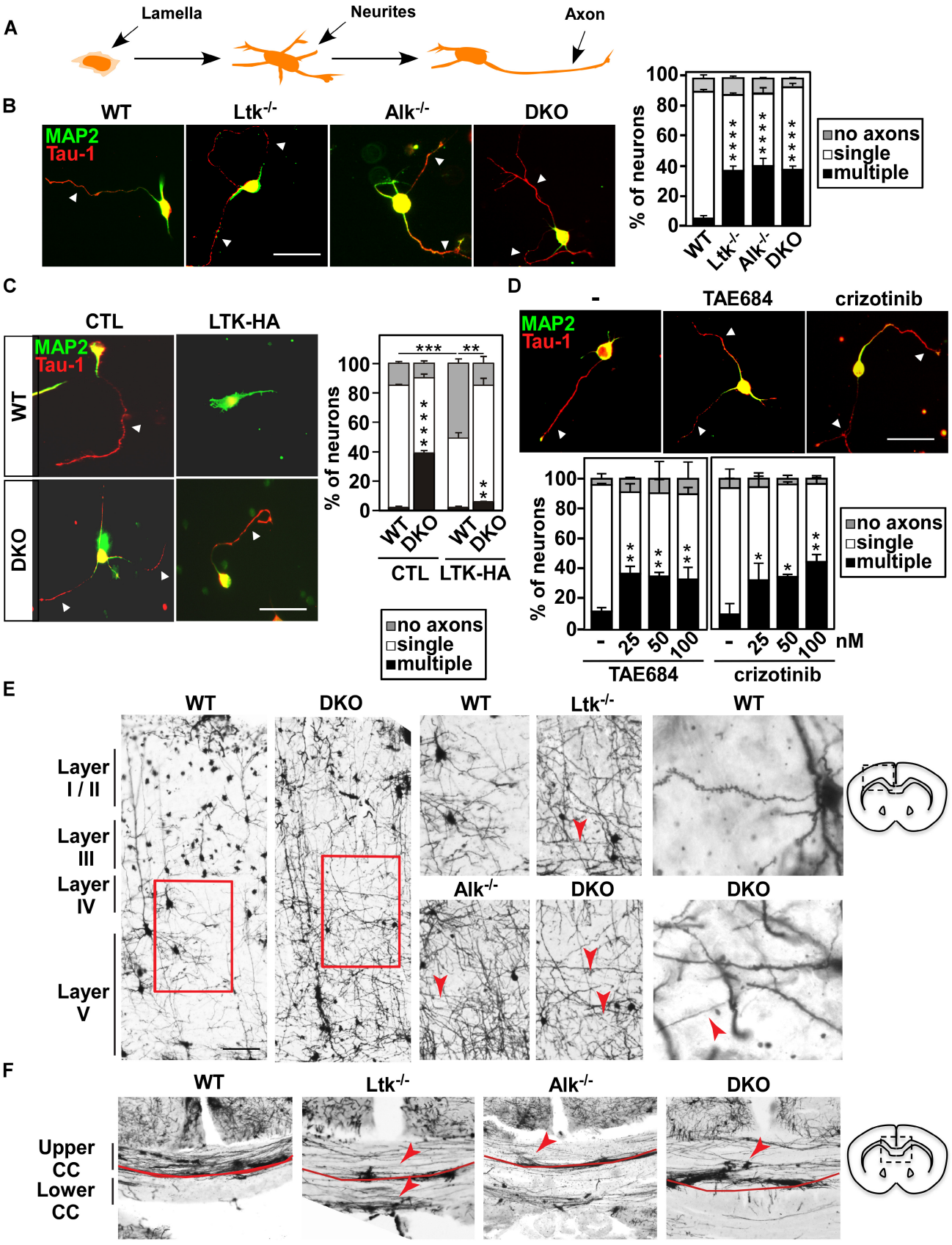


Figure 3.

© 2023 The Authors

Figure 3. Alterations in Ltk and Alk expression or activity disrupt neuronal polarity in cortical neurons and results in defects in neuronal morphology in the brains of knockout mice.

A A schematic illustrating the development of embryonic cortical neurons cultured *in vitro*.

B Dissociated E16 cortical neurons were cultured for 38 h and then fixed. Representative images of cortical neurons from WT, single, or DKO mice, stained for Tau-1, an axonal marker (red), and MAP2, a dendritic marker (green). Arrowheads mark axons. Scale bars are 20 μm.

C Representative images of dissociated WT and DKO cortical neurons, electroporated with plasmids encoding EGFP alone or together with HA-tagged LTK-WT. Cells were fixed 38 h after plating and then stained for Tau-1 (axons, red) and MAP2 (dendrites, green). Arrowheads mark axons. Scale bars are 20 μm. Quantitation of the percent of neurons with multiple, single, and no axons in EGFP-positive neurons is plotted.

D Representative images of WT cortical neurons, treated with the ALK inhibitors, TAE684, and crizotinib or DMSO as a control at 4 h after plating. Neurons were stained for Tau-1 (red) and MAP2 (green). Arrowheads mark axons. Scale bars are 20 μm.

E Golgi stains of adult cortices in wild-type, single ($Ltk^{-/-}$ and $Alk^{-/-}$), and double (DKO) knockout mice show severe defects in neuronal projections and the callosal tract. Representative coronal sections of cortical layers I–V in WT and DKO mice (left), Layers IV–V in WT, single and double knockout cortices (center), and higher magnification images of WT and DKO neurites (right). Examples of disrupted directional growth and extension of projections in pyramidal neurons in knockout mice are marked (red arrowheads). Scale bars are 100 μm.

F Representative coronal sections of the medial region of the corpus callosum in wild-type and mutant cortices. Red line delineates the upper and lower regions of the corpus callosum (CC) with higher axon density within the upper corpus evident in WT mice. Prominent defects in the callosal fibers including substantial deviations and incoherent projections from the major tract in knockout mice compared with WT mice are marked (red arrowheads). Schematics of the regions represented in images are shown on the right. CC, Corpus callosum; Py, pyramidal neurons.

Data information: Data are presented (B–D) as percent of neurons with multiple, single, and no axons and are plotted as the mean ± SEM of 150 neurons per condition from three independent biological experiments. Statistical significance: ****$P < 0.0001$, **$P < 0.01$, *$P < 0.05$ by one-way ANOVA, Dunnett's test.
Source data are available online for this figure.

memory (Miedel *et al*, 2017; Kraeuter *et al*, 2019). Mice were placed in one arm of the Y-maze and exploration of the three arms was monitored for 8 min by video tracking. The number of arms entered and the sequence of entries was recorded. A high alternation rate (degree of arm entries without repetitions) is indicative of sustained cognition as the animals must remember which arm was entered last to avoid re-entry. We found that spontaneous alternations (SAP) and the total number of arm entries by the single $Ltk^{-/-}$ or $Alk^{-/-}$ mice were comparable with wild-types at all ages tested. However, while young (2–3 month) *DKO*s performed similar to wild-type mice, a decrease was observed in older (6- and 12-month-old) *DKO*s (Fig 4B). Thus, young adult mice of all genotypes display normal short-term spatial working memory, with some decline evident in older *DKO* mice.

Finally, to explore executive functions, the puzzle box assay was carried out (Ben Abdallah *et al*, 2011). In this problem-solving test, mice are required to use a range of executive functions including working and contextual memory, spatial navigation, and problem-solving to complete escape tasks (T1–9) of increasing difficulty. Mice must move from a light area to a dimly lit goal box through a tunnel with barriers of increasing complexity introduced over a 3-day period. Repetition of tasks allows assessment of both short-term (T3, T6, T9) and long-term memory (T4 and T7). Analysis of the results revealed that in young mice (2–3 months), *DKO*s displayed an increase in time (latency) of entry to the goal box for all tasks on all 3 days of the experiment as compared to single mutants or wild-type mice (Fig 4C). The latency was notably increased upon the second challenge (T2) when the tunnel door was closed. In young adults (2–3 months), single *Ltk* or *Alk* knockouts showed behaviors similar to WT mice for all tasks, though performance in the most complex tasks (T8 and T9) significantly worsened with age (Appendix Fig S4B and C). Thus, *DKO* mice showed severe deficits in problem-solving behavior that also emerged in aging Ltk and Alk mutant mice for the most complex tasks. No effects on short- or long-term memory were observed in single KO mice, while it was not possible to assess this in *DKO*s who failed all tasks.

Taken together, these behavioral analyses demonstrate that while all genotypes display normal short-term memory, the single $Ltk^{-/-}$ or $Alk^{-/-}$ mice show age-related decline in the performance of complex functions while those lacking both Ltk and Alk, display severe anxiety and are unable to perform tasks requiring executive functions. Thus, the loss of Ltk/Alk disrupts behavior and cognitive functions in adult mice.

The Alkal2 ligand activates Ltk/Alk to control neuronal polarity

We next sought to gain insights into the molecular basis for the disruption of neuronal polarity caused by the loss of *Ltk/Alk*. The Ltk/Alk ligand, Alkal2, is expressed at roughly equivalent levels in both WT and *DKO* mice in the embryonic, newborn, and adult brain and in isolated embryonic cortical neurons (Figs EV1G and EV3A) indicating that changes in ligand expression do not explain the phenotype, thus, we next explored whether the ligand has a role in controlling neuronal morphology. Abrogating expression of Alkal2 using validated siRNAs yielded embryonic cortical neurons that displayed the multiple axon phenotype (Figs 5A and EV3B). Alkal2 protein is not commercially available, so to explore the effects of exogenously added ligand, we generated ALKAL2-conditioned media (ACM) from transiently-transfected HEK293T cells as previously described (Guan *et al*, 2015). We first confirmed that the ALKAL2-conditioned media (ACM) was capable of activating LTK/ALK using IMR-32 human neuroblastoma cells that express wild-type ALK (Janoueix-Lerosey *et al*, 2008) by immunoblotting with pY1586-ALK antibodies (Fig EV3C). Treatment of WT cortical neurons with ALKAL2-conditioned medium (ACM) inhibited the formation of axons (Fig 5B) similar to the effect observed upon overexpressing LTK (Fig 3C and Appendix Fig S3B) but, importantly, had no effect in murine *DKO* neurons (Fig 5B). Thus, Alkal2 inhibits axon outgrowth in a manner dependent on the presence of endogenous Ltk/Alk receptors. Taken together, our results show that Alkal2-mediated activation of Alk and Ltk can regulate neuronal polarity.

Lack of Ltk/Alk expression results in excessive PI3K signaling

Phosphatidylinositol-3-kinase (PI3K) activity is a key driver of neuronal polarization as it is required and sufficient for axon

© 2023 The Authors

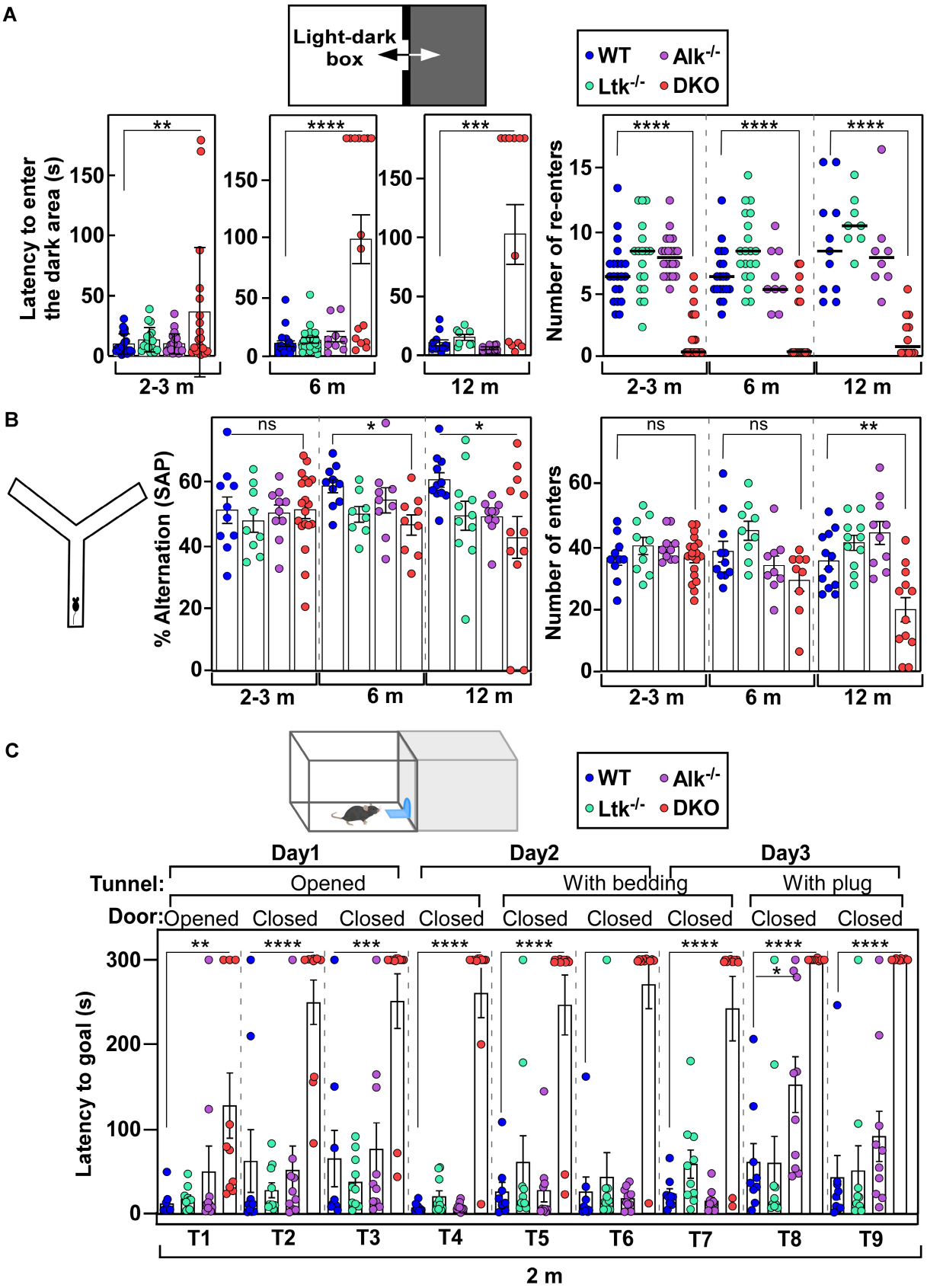


Figure 4.

© 2023 The Authors

Figure 4. DKO mice exhibit behavior abnormalities.

A Schematic of the light–dark box for assessing anxiety levels. Latency to enter the dark box and the number of re-enters into the dark box for each individual mouse of the indicated genotypes and of various ages are plotted.

B Schematic of the Y-maze for assessing working memory. Spontaneous alternation (SAP) and number of arm entries for each individual mouse of the indicated genotypes are plotted.

C Schematic of the puzzle box arena consisting of a white, light compartment (start box) and a black compartment (goal box) divided by black barrier. Latency to reach the goal box during the nine trials of the test is plotted for each individual 2- to 3-month-old mouse of the indicated genotypes.

Data information: Data are plotted as mean ± SEM. Data were analyzed using one-way ANOVA and comparisons with WT were performed using the Dunnett's test (****$P < 0.0001$, ***$P < 0.001$, **$P < 0.01$, *$P < 0.05$; ns, not significant, $n = 8$–20 mice/group, n represents biological replicas).

specification (Yoshimura *et al*, 2006), thus, we next sought to explore whether the loss of Ltk/Alk engages the PI3K pathway. Inhibition of PI3K using the broad specificity inhibitor, LY294002 or with BKM120, a more selective pan-class I PI3K inhibitor that targets all isoforms of the p110 catalytic subunit of PI3K (Maira *et al*, 2012), blocked formation of axons in WT neurons (Fig 5C and D). Remarkably, in neurons isolated from DKO mice, treatment with LY294002 or BKM120 not only prevented the formation of excess axons but restored the wild-type single axon phenotype (Fig 5C and D). Similar results were observed in neurons isolated from single KO mice and in WT neurons in which the expression of Ltk, Alk, or both was abrogated using siRNAs (Fig EV3D and E). The overexpression of the lipid and protein phosphatase, PTEN, which inactivates the PI3K pathway by dephosphorylating PIP3 (Jiang *et al*, 2005), also inhibited the formation of axon-like extensions in wild-type cortical neurons and restored the single axon phenotype in *DKO* neurons (Fig EV3F).

Activation of PI3K results in increased phosphorylation of AKT. Thus, to confirm that the PI3K signaling pathway is activated in the absence of Ltk/Alk, lysates from isolated embryonic cortical neurons, as well as from total brain homogenates from embryonic WT and KO mice were analyzed by immunoblotting using a phospho-specific Akt antibody. These results revealed that isolated neurons and brain extracts from single and/or double knockout mice display increased levels of pAKT (Figs 5E and EV3G). Thus, our results demonstrate that the loss of Ltk/Alk results in excessive PI3K signaling that promotes the formation of multiple axons and that inhibition of PI3K activity can overcome the effects of the loss of Ltk/Alk and restore the normal single axon phenotype in KO neurons.

Igf-1r is activated in Ltk/Alk KO neurons

The observed increase in PI3 kinase activity in KO cortical neurons suggested the possibility that the loss of Ltk/Alk may result in aberrant upstream activation of another receptor tyrosine kinase (RTK), as RTKs are well-known activators of PI3K signaling. Insulin-like growth factor 1 receptor (IGF-1R) is widely expressed in the brain (Fernandez & Torres-Aleman, 2012) and in > 90% of the isolated embryonic E15.5 cortical neurons used in our assays (Appendix Fig S3A), and has been shown to play a role in neuronal polarity, migration and axonal outgrowth (Sosa *et al*, 2006; O'Kusky & Ye, 2012; Nieto Guil *et al*, 2017). Moreover, in ALK-positive lung cancer, the acquisition of resistance to crizotinib is associated with enhanced IGF-1R activation, suggesting that IGF-1R may compensate for reduced ALK signaling during anticancer therapy (Lovly *et al*, 2014). Thus, to test whether IGF-1R is activated in KO neurons, we immunoblotted neuronal lysates using a phospho-tyrosine (pY) antibody that recognizes the autophosphorylation sites in IGF-1R and the closely related Insulin receptor (InsR). This analysis revealed an increase in the levels of phosphorylated Y1135/1136 in cortical neurons in KO mice as compared to wild-type controls (Fig EV4A).

To further explore whether IGF-1R and/or InsR are activated upon loss of Ltk/Alk, we first tested the effect of an inhibitor, tyrphostin, AG1024, which inhibits IGF-1R with 8-fold higher affinity than InsR (i.e., 7 vs. 57 μM, respectively; Parrizas *et al*, 1997), and acts by preventing binding of substrate and ATP. Treatment of cortical neurons with AG1024 at a dose (1 μM) at which only IGF-1R but not InsR was inhibited restored the single axon phenotype in *DKO* neurons (Fig 6A). Similarly, the small toxin molecule, picropodophylin (PPP), which specifically inhibits IGF-1R, but not InsR by blocking phosphorylation of Y1136 and receptor activation (Vasilcanu *et al*, 2004), caused a marked decrease in the number of neurons with multiple axons in both single and double *DKO* cells (Figs 6B and C, and EV4B). Consistent with these observations, treatment of neurons with a neutralizing anti-IGF-1Rα antibody, which prevents binding of the IGF-1 ligand to IGF-1R and thus blocks IGF-1-mediated receptor activation, revealed a restoration of the single axon phenotype in *DKO* neurons (Fig 6C). Finally, siRNA-mediated abrogation of Igf-1r expression in *DKO* cortical neurons switched the multiple axon phenotype into the normal single axon morphology (Fig 6D and E). Of note, in WT neurons, inhibition of Igf-1r receptor activity or silencing of Igf-1r increased the number of neurons with no axons (Fig 6A, B and D), consistent with previous observations demonstrating a role for Igf1-r in neuronal polarity (Sosa *et al*, 2006; Nieto Guil *et al*, 2017). Finally, we examined the effect of inhibiting the Igf1-r on neuronal migration *in vivo*. Remarkably, treatment of DKO embryos with PPP led to a partial restoration of neuronal migration in P2 mice, with some BrdU+ neurons being localized in the superficial layers (Bin 7 and 8; Fig 6F). Of note, in WT mice, PPP treatment blocked the migration of BrdU-labeled neurons (Fig 6F), indicating that Igf-1r activity is required for neuronal migration as previously reported (Nieto Guil *et al*, 2017). Thus, taken together, our results indicate that Igf-1r activity is enhanced upon loss of Ltk/Alk, and this can drive the multiple axon phenotype *in vitro* and drive defects in neuronal migration *in vivo*.

Given that the loss of Ltk/Alk enhances Igf-1r activity, we next examined the effect of activating Igf-1r in the context of wild-type neurons by ectopically adding murine, recombinant IGF-1. Cortical neurons treated with IGF-1 formed multiple axons in a dose-dependent manner (Fig EV4C), with the effect of 50 nM IGF-1 being similar to that observed for untreated *DKO* cortical neurons (Figs 5G and EV4C). By contrast, neither insulin (a ligand for InsR/IGF-1R) nor EGF (a ligand for EGFR) altered the number of axons and axon-

© 2023 The Authors

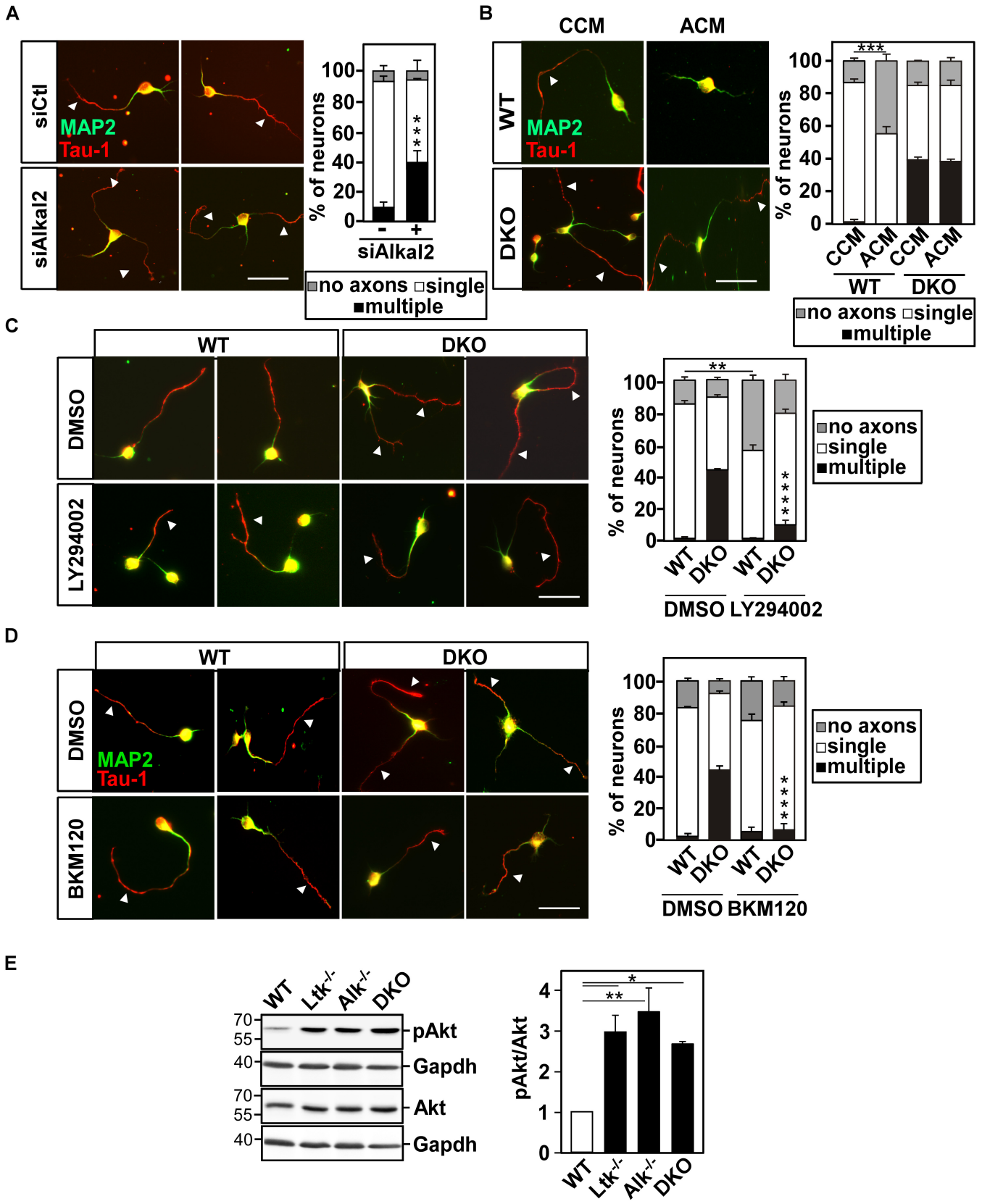


Figure 5.

© 2023 The Authors

Figure 5. Analysis of the effects of ligand and inhibition of PI3 kinase activity on neuronal polarity.

A-D Representative images of cortical neurons fixed at 38 h and stained with Tau-1 (axons, red) and MAP2 (dendrites, green) are shown. Arrowheads mark axons. Scale bars are 20 μm. (A) RNAi-mediated depletion of Alkal2 in WT cortical neurons disrupts neuronal polarity. Dissociated E16 WT cortical neurons were transfected with siAlka2 or siCTL. (B) ALKAL2 ligand addition modulates neuronal polarity. WT and DKO cortical neurons were treated with control (CCM) or ALKAL2 (ACM)-conditioned medium, 4 h after plating. (C, D) Treatment of cortical neurons from WT or KO mice with PI3 kinase inhibitors reverses polarity defects caused by loss of Ltk/Alk. Dissociated E16 cortical neurons were treated with LY294002 (10 μM; C), BKM120 (1 μM; D), or DMSO control, 4 h after plating.

E A representative immunoblotting showing the levels of pAKT (pAkt^{S473}), Akt, and GAPDH (loading control) in lysates of cortical neurons from WT, single, and DKO mice. Quantitation of pAkt^{S473} to Akt levels relative to WT is plotted.

Data information: In (A–D) quantitation of the percent of neurons with multiple, single, or no axons is plotted as the mean ± SEM of $n = 150$ neurons per condition from 3 (A-, B-, C-WT) or 4 (C-DKO, D) independent biological experiments. Statistical significance: ****$P < 0.0001$, ***$P < 0.001$, **$P < 0.01$ by one-way ANOVA, Dunnett's test (E), or Student's *t*-test (A–D).
Source data are available online for this figure.

like neurites (Figs 6G and EV4C). The effect of IGF-1 was completely abolished by pretreatment of cells with the IGF-1R inhibitor, PPP, consistent with the notion that activation of Igf-1r leads to the formation of multiple axons (Fig 6G). In *DKO* cortical neurons addition of IGF-1, however, did not increase further the number of neurons bearing multiple axons, suggesting that Igf-1r activity is already saturated in *DKO* neurons (Figs 6G and EV4C). Altogether, these data provide compelling evidence that Igf-1r is activated in cortical neurons upon loss of Ltk/Alk and that this increases PI3 kinase activity to promote the formation of multiple axons. Our results also show that pharmacologically blocking IGF-1R activity or abrogating Igf-1r expression can restore the normal single axon phenotype in KO cortical neurons.

Ltk/Alk modulates Igf-1r levels and activity

We next conducted studies to explore the molecular mechanism that would lead to increased Igf-1r activity in KO neurons. Analysis of Igf-1r mRNA expression by real-time PCR revealed no differences in WT versus KO cortical neurons (Fig EV4D) indicating a post-transcriptional mechanism. We next examined Igf-1r protein levels and activity by immunoblotting using antibodies that recognize Igf-1r total protein or the phosphorylated (pY1135/1136), activated Igf-1r/InsR. This revealed that *DKO* cortical neurons display a modest increase in total Igf-1r protein levels (< 2 fold) along with a more dramatic enhancement in the levels of activated Igf-1r as compared to WT controls even when corrected for the increase in protein levels (Fig 7A). Thus, the increase in Igf-1r activity in KO cortical neurons is not a result of transcriptional regulation but rather due to post-transcriptional enhancement of the levels of both total protein and activated receptors.

To determine how Ltk/Alk might modulate Igf-1r, we explored whether Ltk/Alk forms a complex with Igf-1r. When transiently overexpressed in HEK293T cells, an association between IGF-1R and either LTK or ALK was detected (Fig EV4E and F). In LTK expressing T-REx stable cells, the interaction of endogenous IGF-1R with Dox-induced Flag-tagged LTK was also observed (Fig 7B). This interaction was substantially reduced when a kinase-inactive variant (KR) of LTK was used, indicating that the association requires active LTK (Fig EV4G). By contrast, IGF-1R kinase activity was unnecessary for efficient interaction with LTK (Fig EV4H). To examine whether LTK/ALK might phosphorylate IGF-1R, we performed an *in vitro* kinase assay using recombinant proteins, comprised of the kinase domain alone of LTK (GST-LTK) and the kinase and C-terminal tail of IGF-1R (His-IGF-1R). The addition of GST-LTK increased the level of phosphorylation on IGF-1R over the basal levels of IGF-1R autophosphorylation, indicating that LTK can phosphorylate IGF-1R (Fig 7C). A GST pulldown assay confirmed that the kinase domain of LTK was sufficient for interaction with the kinase/C-terminal region of IGF-1R (Fig EV4I). Next, we analyzed IGF-1R phosphorylation in HEK293T cells transiently transfected with Flag-tagged IGF-1R with or without HA-tagged WT or KR variants of LTK. IGF-1R was immunoprecipitated and subjected to an *in vitro* kinase assay. Consistent with the assay using recombinant proteins, IGF-1R is phosphorylated by WT but not kinase-inactive LTK (Fig 7D). IMR-32 cells express both endogenous ALK and IGF-1R, thus we examined the effect of ligand on receptor interactions. Immunoprecipitation of ALK revealed an association with IGF-1R that was dependent on treatment with ALKAL2 (ACM)-conditioned media, confirming the importance of ligand-induced activation of ALK for the interaction with IGF-1R (Fig 7E). Finally, pulldown assays from embryonic mouse brain lysates using bacterially expressed recombinant GST-tagged kinase domains of active ALK or LTK showed efficient isolation of endogenous Igf-1r (Figs 7F and EV4J), confirming the association and indicating that the kinase domain of LTK/ALK is sufficient for this interaction. Taken together, these findings support the notion that active LTK/ALK interacts with and phosphorylates IGF-1R.

Given the increased level of active Igf-1r and since receptors signal from the plasma membrane, we next examined whether the presence of Ltk/Alk might modulate the levels of Igf-1r on the cell surface. For this, cell-surface proteins were biotinylated, cells were lysed, biotin-labeled proteins were collected with NeutrAvidin-Sepharose beads and bound proteins were then detected by immunoblotting. In dissociated cortical neurons, we observed that the levels of cell-surface-localized Igf-1r were significantly increased in neurons from *DKO* mice when compared to WT neurons (Fig 7G). In the converse experiment using T-REx cell stably expressing doxycycline (DOX)-inducible LTK, we observed that increasing LTK expression resulted in a decrease in cell-surface localization of endogenous IGF-1R (Fig 7H). Thus, LTK/ALK attenuates cell-surface expression of IGF-1R and accordingly loss of Ltk/Alk enhances cell-surface localization of Igf-1r.

We next examined the effect of Ltk/Alk receptor activation on Igf-1r cell-surface expression and protein levels in WT neurons. For this, cell-surface receptors on cortical neurons were labeled with biotin, and cells were then incubated at 37°C for varying times with control (CCM) or ALKAL2 (ACM)-conditioned media to activate Ltk/Alk. Remarkably, after 30 min of treatment with ACM, a 50% reduction in Igf-1r on the cell surface was observed, indicating a

© 2023 The Authors

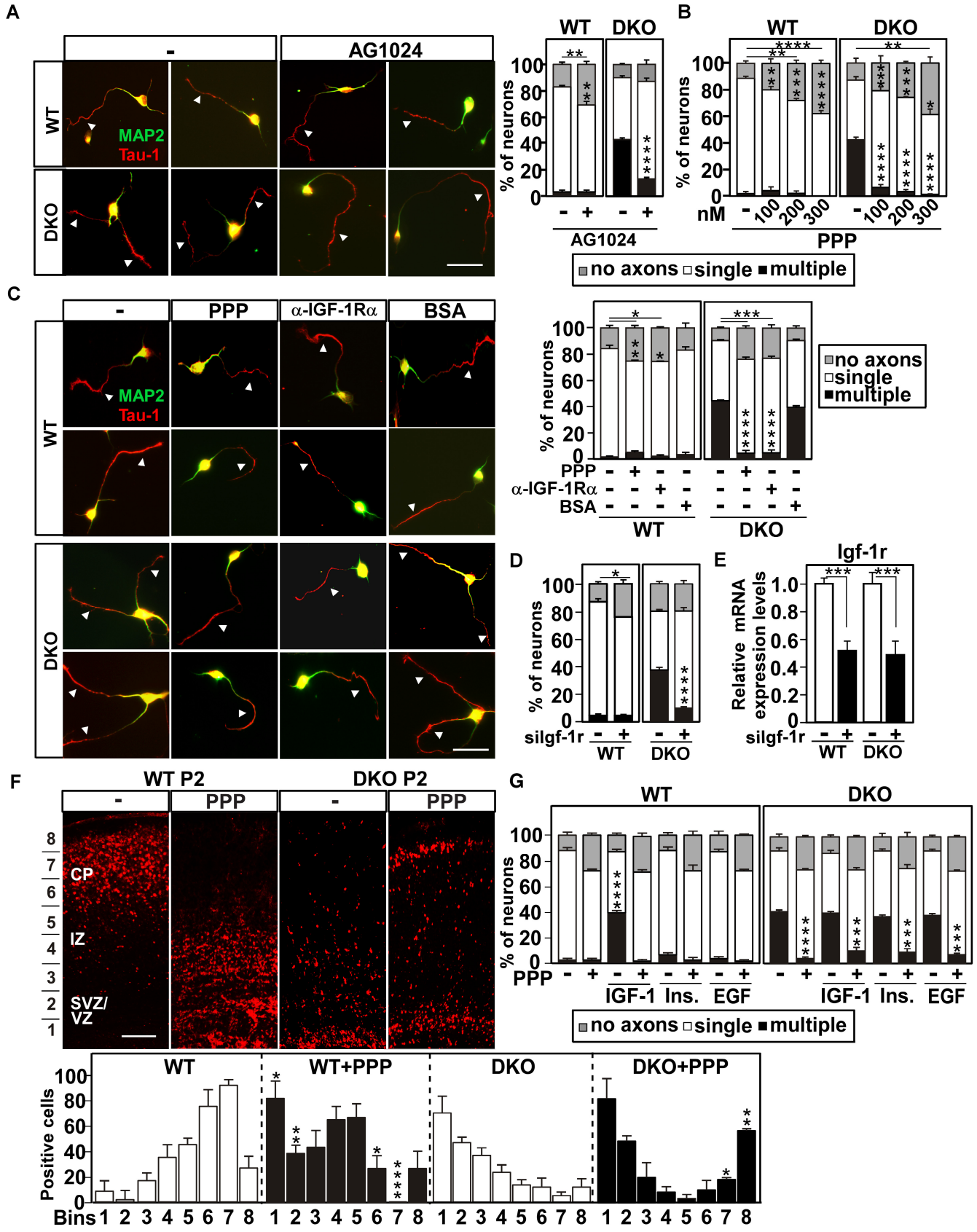


Figure 6.

© 2023 The Authors

Figure 6. Loss of Ltk/Alk promotes Igf-1r activity.

A, B IGF-1R inhibitors rescue the multiple axon phenotype in DKO cortical neurons. Cortical neurons, isolated from WT and DKO mice were treated with 1 μM AG1024 (A), varying concentrations of Picropodophylin (PPP; B) or DMSO as control 4 h after plating, fixed at 38 h, and stained for Tau-1 (axons, red) and MAP2 (dendrites, green). Arrowheads mark axons. Scale bars are 20 μm. Quantitation of the percent of neurons with multiple, single, or no axons is plotted.

C Blocking Igf-1r activation with a neutralizing anti-IGF-1Rα antibody rescued the multiple axon phenotype in DKO cortical neurons. Neurons isolated from WT or DKO mice were treated with anti-IGF-1Rα antibody (1.5 μg/ml), BSA as control (1.5 μg/ml), or PPP (200 nM) 4 h after plating. Representative images of Tau-1 and MAP2 stained cells with arrowheads marking axons are shown. Scale bars are 20 μm. Quantitation of the percent of neurons with multiple, single, or no axons is plotted.

D Reduced expression of Igf-1r restores normal neuronal morphology in DKO cortical neurons. Cortical neurons isolated from WT and DKO mice were electroporated with siIgf-1r together with a GFP plasmid to mark transfected cells. Neurons were fixed at 36 h and stained for Tau-1 and MAP2. Quantitation of the percent of neurons with multiple, single, and no axons in EGFP-positive neurons is plotted.

E Knockdown efficiency was confirmed by qPCR.

F Inhibition of Igf-1r blocks neuronal migration *in vivo*. Pregnant E14 WT or DKO mice were injected (i.p) with BrdU and 24 h later were injected with PPP or saline as control. Brains from P2 pups were subjected to staining with anti-BrdU antibody. Quantitation in P2 cortices of BrdU-positive cells in the indicated bins (marked on left) is plotted. The location of the cortical plate (CP), intermediate zone (IZ), and subventricular/ventricular zone (SVZ/VZ) in P2 mice are indicated. Scale bars are 50 μm.

G Analysis of the effect of ectopically applied recombinant IGF-1. Cortical neurons isolated from WT or DKO mice were treated with PPP (200 nM), DMSO as control, and/or IGF-1 (50 nM), insulin (100 nM), or EGF (20 ng/ml). Cells were fixed at 38 h and stained for Tau-1 and MAP2. Quantitation of the percent of neurons with multiple, single, or no axons is plotted.

Data information: Data are presented as the mean ± SEM, $n \geq 150$ neurons per condition from 4 (A, B) or 3 (C, D, G) independent biological experiments. Data in (E) are presented as the mean ± SEM from three independent experiments, each with three technical replicates. Data in (F) are presented as the mean ± SEM from 3 (DKO) and 2 (WT) independent biological experiments. Statistical significance: ****$P < 0.0001$, ***$P < 0.001$, **$P < 0.01$, *$P < 0.05$ by one-way ANOVA, Dunnett's test (A–F, G), or Student's *t*-test (F), where WT vs. WT + PPP or DKO vs. DKO + PPP were compared.
Source data are available online for this figure.

more rapid internalization of Igf-1r in the presence of active Ltk/Alk (Fig 7I). Consistent with the observed decrease in cell-surface Igf-1r upon activation of Ltk/Alk, the addition of Igf-1 had no effect on axon formation in neurons in which Ltk/Alk receptors had been previously activated by ALKAL2 (Fig 7J). Thus, ligand-induced activation of Ltk/Alk favors Igf-1r internalization and results in a decrease in Igf-1r cell-surface expression.

Taken together, our results reveal a key role for Ltk/Alk in controlling neuronal morphology and patterning of the cortex and provide a molecular model for how Ltk/Alk functions in this context (Fig EV5). Specifically, Alkal2-activated Ltk/Alk act to limit the level of cell-surface and activated Igf-1r by promoting Igf-1r internalization to maintain proper neuronal morphology. Loss of Ltk/Alk increases Igf-1r cell-surface localization and activity, to enhance PI3K signaling and thereby promotes the formation of multiple axons. *In vivo*, the loss of Ltk/Alk disrupts neuronal polarization, delays neuronal migration and cortical patterning and in adults leads to an aberrant morphology of cortical neurons, and disrupts axon tracts in the corpus callosum. Altogether, this highlights a key role for Ltk/Alk in cortical development and patterning.

Discussion

The establishment of axon-dendrite polarity is fundamental for the radial migration of neurons during mammalian cortical development and subsequently for the proper formation of the neuronal circuitry. Here, we demonstrate that the receptor tyrosine kinases, Ltk and Alk, contribute to the polarization of developing neurons and the subsequent timing of cortical patterning. We observed that Ltk, Alk, and the Ltk/Alk ligand, Alkal2, are expressed in the developing cortex, including in the embryonic progenitor cell populations found in the ventricular and subventricular zones, where neuronal polarization occurs. Cortical neurons exhibit the highest migratory activity between E14.5 and E16.5, which also continues in newborn pups, up to P7 (Chen *et al*, 2008). Proper neuronal morphology is essential for neuronal migration and in line with this, we observed that in Ltk and Alk single or double knockouts (*DKOs*), the radially migrating cortical neurons in E17.5 and newborn pups display a delay in localization to the correct position within the defined layers of the developing cortex.

Consistent with the *in vivo* observations, our analysis of isolated primary embryonic neurons confirmed that loss or inhibition of Ltk/Alk activity using siRNAs or small molecule inhibitors or in embryonic neurons extracted from KO mice, there are defects in neuronal polarization. These neurons display the presence of multiple axons, a phenotype that was rescued by the overexpression of Ltk/Alk. Of the two known and related Ltk/Alk ligands (Reshetnyak *et al*, 2015), only Alkal2 was expressed in the developing and adult cortex. Consistently, a deficiency in Alkal2 expression or activation of Ltk/Alk receptors by the addition of exogenous ALKAL2, yielded neuronal phenotypes resembling those of abrogated or overexpressed Ltk/Alk receptors, respectively, thereby highlighting the functional link of ligand-mediated receptor activation in the regulation of neuronal morphology. As the ligands for Ltk/Alk have only recently been discovered, many aspects of precisely how these secreted small proteins act remain to be determined. As positively charged, unstable proteins, the ligands are likely to act locally and may act in an autocrine fashion (Ahmed *et al*, 2022; Defaye *et al*, 2022), which is consistent with our findings that abrogation of ALKAL2 expression in the cortical neurons, which also express the LTK/ALK receptors, blocked axon outgrowth. Whether ALKAL2 is also expressed in other CNS cell types that can act to modulate axon outgrowth warrants future investigations. Similarly, since we used constitutive rather than conditional knockouts of ALK and LTK for our studies, it is also possible that loss of LTK/ALK in non-neuronal cell types, such as radial glia cells, may have contributed to some of the observed phenotypes, such as the observed delay in neuronal migration.

© 2023 The Authors

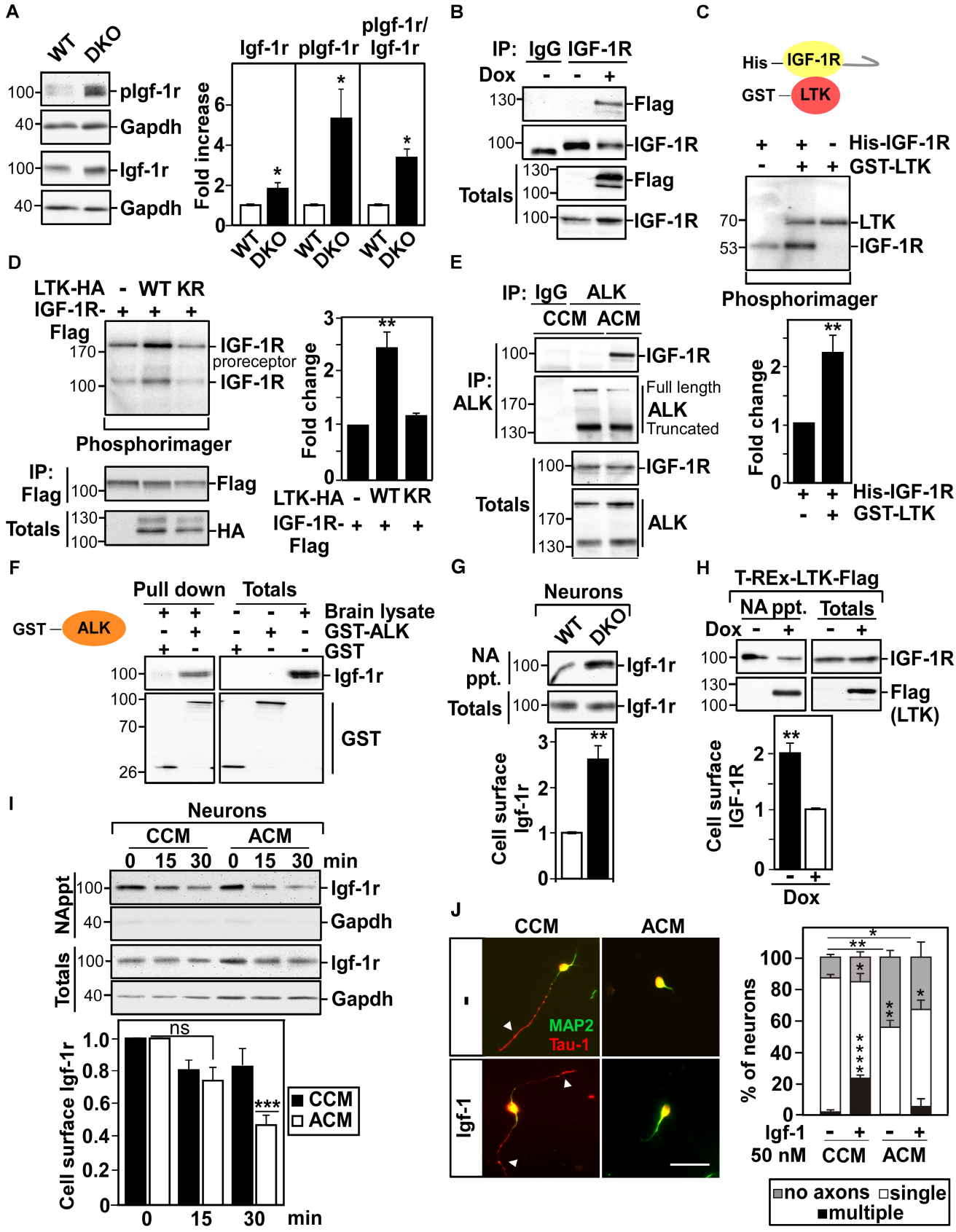


Figure 7.

© 2023 The Authors

Figure 7. Ltk/Alk interacts with and modulates Igf-1r stability and cell-surface expression.

A Representative immunoblot showing the levels of phosphorylated (pIgf-1r$^{Y1135/1136}$), total Igf-1r, and Gapdh (as loading control) in lysates of isolated cortical neurons from WT and DKO mice. Band intensities for Igf-1r were normalized to Gapdh (left plot) and for pIgf-1r were normalized either to Gapdh (middle plot) or to Igf-1r (right plot) and the fold increase relative to WT is plotted.

B Endogenous IGF-1R was immunoprecipitated from cell lysates of T-REx cells, treated without (−) or with (+) doxycycline (Dox) to induce expression of Flag-tagged LTK and the interaction with LTK-Flag was visualized by immunoblotting.

C Representative image showing phosphorylation of recombinant His-tagged IGF-1R (kinase domain and C-terminal region) by recombinant GST-LTK (kinase domain) in an *in vitro* radioactive kinase assay. Phosphorylation of IGF-1R was quantitated as fold change relative to autophosphorylation of IGF-1R alone.

D Representative image showing the phosphorylation of IGF-1R by co-expressed WT or Kinase-deficient (KR) LTK in *in vitro* radioactive kinase assay. The levels of immunoprecipitated IGF-1R and total LTK-HA were visualized by immunoblotting (bottom). Phosphorylation of IGF-1R was quantitated as fold change relative to autophosphorylation of IGF-1R alone.

E Endogenous ALK was immunoprecipitated from lysates of IMR-32 cells, treated with control (CCM) or ALKAL2 (ACM)-conditioned media, and co-precipitated endogenous IGF-1R was detected by immunoblotting.

F Homogenates from WT embryonic brains were incubated with GST-ALK or GST alone, and immobilized to GSH-Sepharose beads. Bound and total proteins were subjected to immunoblotting with anti-IGF-1R antibody.

G Cell-surface expression of Igf-1r has increased in DKO cortical neurons. Cell-surface Igf-1r (NA ppt) is normalized to totals and the fold change relative to WT samples is plotted.

H LTK decreases cell-surface expression of IGF-1R in T-Rex-LTK stable cells. Cell-surface IGF-1R (NA ppt) normalized to totals as fold change relative to samples expressing LTK (+Dox) is plotted.

I WT cortical neurons were labeled with biotin and incubated at 37°C for 15 or 30 min in the presence of CCM or ACM-conditioned media. Cell-surface Igf-1r (NA ppt) normalized to totals as the fold change relative to controls at time 0 is plotted.

J WT and DKO cortical neurons were treated with control (CCM) or ALKAL2 (ACM)-conditioned medium 4 h after plating and IGF-1 was added 1 h later. Representative images of cells fixed at 36 h and stained for Tau-1 (axons; red) and MAP2 (dendrites: green) are shown. Arrowheads mark axons. Scale bars are 20 μm.

Data information: Data are presented as the mean ± SEM from 3 (A, G, H) or 4 (I) independent experiments. Representative blots from three independent biological experiments are shown in (A, B, E–G). Data in (C, D) are plotted as the mean ± SEM from 6 (C), 7 (D), or 3 (D for LTK-KR) independent biological experiments. In (J) quantitation of the percent of neurons with multiple, single, or no axons is plotted as the mean ± SEM of $n = 150$ neurons per condition from three independent experiments. Statistical significance: ****$P < 0.0001$, ***$P < 0.001$; **$P < 0.01$; *$P < 0.05$ by the Student's *t*-test.
Source data are available online for this figure.

During the course of our experiments, we observed that loss of either Ltk or Alk alone or both together yielded a similar proportion of isolated neurons with a multiple axon phenotype. Our single-molecule RNA *in situ* analysis demonstrated that the bulk (~70%) of isolated neurons express both Ltk and Alk, as well as Igf-1r. These results, thus, indicate that in embryonic neurons Ltk or Alk cannot compensate for loss of the other, rather that both Ltk and Alk are required to regulate neuronal polarity. We made similar observations *in vivo*, where loss of either Ltk or Alk alone or both together, resulted in defects in neuronal migration and cortical patterning. Taken together, these data lead us to speculate that Ltk and Alk may act together in the context of a heteromeric Ltk/Alk complex to regulate neuronal polarity (Fig EV5). While recent structural insights into ligand-mediated receptor activation have focused on ALK or LTK homodimers (Reshetnyak *et al*, 2021), the formation of heteromeric Ltk/Alk complexes in the presence of a ligand has been previously reported (Guan *et al*, 2015).

The mouse brain continued to develop postnatally and, interestingly, the impaired cortical layering present at birth, showed improvements by P7, and appeared resolved by adulthood. However, it is worth noting that despite the apparent recovery of normal cortical patterning, adult mice display neurons with morphological defects including the presence of aberrant neuronal projections within the cortex. In addition, there is a disruption of the axon tracts within the corpus callosum, which are derived primarily from neurons from cortical layers II-V. While we have not directly demonstrated that the defects in the axon tracts are the result of excess Igf1-r activity, it is known that defects in the corpus callosum can arise from earlier disruptions in neuronal polarization (Edwards *et al*, 2014), indicating that the aberrant axon tracts may be the result of effects on neuronal morphology. Consistent with the presence of alterations in adults, *DKO* mice display behavioral anomalies including severe anxiety and the inability to perform complex tasks requiring executive functions. In general, the single $Ltk^{-/-}$ or $Alk^{-/-}$ mice behaved similar to WT though an age-related decline in the performance of complex functions was observed. This suggests that in single mutant adults, compensatory mechanisms such as re-wiring of neuronal circuits can overcome the severity of the defect. It is also possible that there are Igf1-r independent, but redundant Ltk/Alk pathways that result in the behavioral defects only observed in the DKOs, such as the recently reported ALK-LIMK-cofilin pathway, which regulates synaptic scaling (Zhou *et al*, 2021). Interestingly, in the Golgi-stained sections (Fig 3E), we noticed that there appeared to be a reduction in the number of dendritic spines in DKO versus WT mice. As disrupted spines can impact behavior, future studies directed at exploring alterations in spine formation or numbers could provide additional insights into the behavioral and cognitive differences observed in knockout adult mice. It is worth noting that in mice deficient in Alk alone, others have reported subtle behavioral alterations, altered responses to ethanol and hypogonadotropic hypogonadism (Bilsland *et al*, 2008; Lasek *et al*, 2011; Weiss *et al*, 2012; Witek *et al*, 2015).

Our mechanistic investigations in cultured neurons revealed that the presence of additional axons was due to excess PI3 kinase activity resulting from the activation of Igf-1r signaling that occurred upon the loss of Ltk/Alk (Fig EV5). Consistent with these studies, administration of a small molecule inhibitor of Igf-1r *in vivo* partially rescued the neuronal migration defects observed in Ltk/Alk knockout mice indicating excess Igf-1r activity also contributes to the migrational delay. IGF-1R belongs to the subfamily of insulin transmembrane receptor tyrosine kinases, is widely expressed in the brain, and has a well-studied role in neuronal polarity, migration, and axonal outgrowth (Sosa *et al*, 2006; O'Kusky & Ye, 2012; Nieto Guil *et al*, 2017). Activation of IGF-1R engages the PI3 kinase

© 2023 The Authors

signaling pathway, which leads to the accumulation of PIP3 in the growth cone that in turn is critical for regulating membrane expansion and axonal outgrowth (Laurino *et al*, 2005; Sosa *et al*, 2006). In line with this, we showed that increased PI3K activity as a result of the loss of Ltk/Alk could be attributed to an increase in Igf-1r cell-surface localization and activity. Ligand-induced activation of Ltk/Alk in WT neurons resulted in a loss of biotin-labeled cell-surface Igf-1r, which is strongly indicative of increased internalization. Since internalization can lead to receptor degradation, this is consistent with our observation of a post-transcriptional increase in Igf-1r protein levels upon loss of Ltk/Alk. It is worth noting that changes in cell-surface expression of Igf-1r, have also been reported to occur through exocytosis and that this process is essential for membrane expansion during axon formation (Quiroga *et al*, 2018). Thus, the increase in cell-surface expression of Igf1-r in DKO neurons may also be explained by enhanced exocytosis. In either case, the consequent multi-axon phenotype could be prevented using pharmacological inhibitors of Igf-1r, siRNAs targeting Igf-1r, or neutralizing anti-IGF-1Rα antibodies. The compensatory upregulation of Igf-1r upon loss of Ltk/Alk activity is strikingly similar to reports that chronic inhibition of ALK in non-small-cell lung cancer (NSCLC) patients leads to the upregulation of Igf1-r activity (Lovly *et al*, 2014). Our studies further revealed that Ltk/Alk interacts with Igf-1r in a manner that is dependent on Ltk/Alk activation, that Ltk/Alk can promote phosphorylation of Igf-1r, and that this interaction results in a decrease in cell-surface expression and signaling of Igf-1r. RTKs are subject to numerous phosphorylation events, some of which are critical for receptor trafficking. In the case of Igf-1r, identifying and characterizing these events is an ongoing, active field of investigation (Rieger & O'Connor, 2020), with a recent study reporting that Y1250 phosphorylation promotes Igf-1r internalization (Rieger *et al*, 2020). Thus, the precise details of how Ltk/Alk mediated phosphorylation of Igf-1r promotes loss of cell-surface Igf-1r remains to be determined.

Altogether, our work uncovers a new role for Ltk/Alk as regulators of neuronal polarity and migration and indicates that correct neuronal morphology requires tightly regulated activity and expression of Ltk/Alk and their ligand. Aberrant activation of ALK due to protein fusions, point mutations, and overexpression have been described in many cancers (Palmer *et al*, 2009; Hallberg & Palmer, 2016) and a recent study provided compelling evidence that the overexpression of the ligand, ALKAL2 in mice can drive neuroblastoma (Borenas *et al*, 2021). ALK inhibitors are in use in the clinic for the treatment of a variety of ALK-driven tumors, including NSCLC, primarily occurring as aberrant fusion proteins since ALK/LTK are not normally expressed in the lung. Second- and third-generation ALK inhibitors, such as ceritinib, alectinib, brigatinib, and lorlatinib have been designed to cross the blood–brain barrier as a means to treat the frequently observed brain metastasis in ALK-driven NSCLC tumors treated with crizotinib (Awad & Shaw, 2014; Chuang & Neal, 2015). Interestingly, a phase 2 clinical trial for lorlatinib showed that about 39% of patients (of 275 in the trial) displayed CNS effects that included changes in cognitive function, mood, and speech (Solomon *et al*, 2018). Thus, our study could provide mechanistic insights into the basis for these adverse effects and further suggests that co-treatment with IGF-1R inhibitors may be a route for mitigating these effects. As the development of resistance in tumors to virtually all kinase inhibitors is inevitable, our study also provides a potential therapy whereby co-treatment with IGF-1R inhibitors may impact the outcome. Our findings may also raise awareness for the use of ALK inhibitors for cancer treatment of females during pregnancy or lactation or in infant and young cancer patients and suggest that more considerations should be given to the potential risk of adverse complications during brain development.

Materials and Methods

Animals

All animal experiments were performed in accordance with the Animal Care and Use Committee of the University of Toronto. Mice were group-housed (up to 4 per cage) with temperature controlled at 21–22°C and with 12-h light–dark cycles. Animals were given food and water *ad libitum*. Wild-type CD-1 and C57BL/6 mice were purchased from Charles River and mutant animals were bred in house. $Alk^{-/-}$ and $Ltk^{-/-}$ knockout mice were generous gifts from Dr. Stephen Morris (St-Jude CRH, Memphis) and Dr. Joseph Weiss (OHSU, Oregon), respectively. $Alk^{-/-}Ltk^{-/-}$ double knockout animals were generated by crossing homozygous $Alk^{-/-}$ and $Ltk^{-/-}$ single knockout mice. Genotyping was performed by PCR analysis using primers listed in Appendix Table S1. Mutant *Ltk* and *Alk* alleles produced a band of 400 base pairs in PCR and the wild-type allele produced a 500 base pair product.

Antibodies, reagents, cDNA constructs, and siRNAs

All primary antibodies used in the study are listed in Appendix Table S2. The following secondary antibodies and dyes were used: Alexa Fluor (488, 546, 594, 647, goat anti-mouse IgG1 cross-adsorbed Alexa Fluor 488 or 350 and anti-mouse IgG2a cross-adsorbed Alexa Fluor-568), phalloidin-rhodamine and 4′, 6-diamidino-2-phenylindole (DAPI) from ThermoFisher; anti-mouse IgG-horse radish peroxidase (HRP), anti-rabbit IgG-HRP and anti-rat IgG-HRP from Jackson Laboratories. The pcDNA3-FAM150B-HA plasmid, encoding ALKAL2 (FAM150B; Guan *et al*, 2015) was a gift from Ruth Palmer (University of Gothenburg, Sweden). LTK, ALK, and IGF-1R constructs were generated using the Gateway system (Life Technologies) by transferring from the Gateway entry clone vector into C-terminally-tagged pCMV5-based destination vectors. LTK-K544R and IGF-1R-K1003R mutants were generated by PCR-mediated site-directed mutagenesis. For gene silencing experiments, siRNA for Ltk, Alk, Igf-1r, Alkal2, and RNAi-negative control were purchased from Dharmacon (siCTL-ON TARGET plus Nontargeting siRNA #3 D-001810-03; siAlk-siGenome Mouse Alk (111682) siRNA, set of 4, MQ-0401104-01; siLtk-siGenome Mouse Ltk, D-063855-04; siIgf-1r-siGenome mouse Igf-1r (16001), set of 4, MQ-056843-01; siAlkal2-siGenome mouse Fam150b (100294583) siRNA, set of 4, MQ-042520-00). All siRNAs targeting a single gene were used as a pool of validated individual siRNAs. Individual siRNAs were validated in primary cortical neurons by confirming the knockdown efficiency of each of the four individual siRNA present in the original pool of four as compared to a nontargeting control siRNA. New pools of siRNA were generated from highly efficient individual siRNAs (siAlk: si1 + 2 + 4, siLtk: si1 + 4,

 © 2023 The Authors

siAlkal2: si1 + 4, si Igf-1r: si2 + 3 + 4) and were used in experiments.

Cell culture and transfections

Human embryonic kidney cells HEK 293T were obtained from American Type Culture Collection (ATCC) and cultured in DMEM supplemented with 10% fetal bovine serum (FBS, Gibco). T-REx-LTK stable cells, expressing Doxycycline-inducible Flag-tagged LTK, were generated by Gateway cloning (Invitrogen) and were grown in DMEM supplemented with 10% FBS, 1% penicillin/streptomycin (Gibco), 200 μg/ml hygromycin B (Invitrogen) and 3 μg/ml blasticidin S HCl. Human neuroblastoma IMR-32 cells were a gift from Igor Stagljar (CCBR, Toronto) and were maintained in MEM Eagle medium (Sigma), supplemented with 10% FBS, 1% nonessential amino acids (NEAA, Gibco), and 1% sodium pyruvate (Gibco). Cell lines were maintained at 37°C in a humidified atmosphere at 5% CO_2. All cell lines were monitored for mycoplasma contamination using the MycoAlert mycoplasma detection kit (Lonza). Transfection of HEK 293T cells was performed using the calcium phosphate method. Media was replaced 24 h later and at 44 h post-transfection, cell lysates were collected and subjected to immunoblot analysis or co-immunoprecipitation using antibodies listed in Appendix Table S2.

Primary murine cortical cell cultures, transfection, and measurement of neurite lengths

Primary cortical neurons were obtained from E16 to 16.5 mouse embryos as previously described (Xu *et al*, 2004). Briefly, embryonic brains were collected in Hank's balanced salt solution (HBSS, Gibco). Cortices were dissected into small pieces and digested in 0.25% trypsin (Sigma), and the reaction was stopped by the addition of DMEM supplemented with 10% FBS. Tissues were then mechanically dissociated into a single cell suspension with a glass pipette, which was then filtered through cell strainer. Dissociated primary cortical neurons were plated on tissue culture plates or chambers, coated with poly-L-lysine (20 μg/ml, Sigma) and laminin (2 μg/ml). Neurons were cultured in serum-free Neurobasal medium (Gibco) supplemented with 2% B27 (Invitrogen), 1% N2, L-glutamine, 50 IU/ml penicillin, and 50 μg/ml streptomycin.

Transfection of dissociated neurons was performed using the AMAXA Nucleofector system (program O.005) with the mouse neuron Nucleofector kit (Lonza) following the manufacturer's specifications. Briefly, $3–5 \times 10^6$ cells were transfected with 2 μg GFP expressing plasmid (EGFP) as a reporter and 4 μg of plasmid DNA or 50 nM of siRNAs. All DNAs were prepared using Endo Free Maxiprep kit (Qiagen). Media was replaced 3 to 4 h after plating. For quantification, neurons were stained for Tau-1 (axonal marker) and MAP2 (dendritic marker) and neurites; positive for Tau-1 and negative for MAP2 were considered axons. In experiments where an axonal marker was not used (i.e., Tuj1, phalloidin, GFP), an axon was defined as the longest neurite that was 3.5 times longer than the diameter of the soma. All measurements were performed using Volocity software (Perkin Elmer). Data are expressed as percentage of all neurons for a minimum of 100 neurons per condition from three independent experiments unless otherwise indicated.

Small molecule inhibitors and ligand stimulation

Cortical neurons were treated with inhibitors or ligands 4 h after plating and were fixed 33–38 h after treatment for analysis. For IGF-1R, inhibitors or activators were added in starvation medium (serum-free Neurobasal medium, supplemented with 2% B27 minus insulin, 1% L-glutamine, 50 IU/ml penicillin, and 50 μg/ml streptomycin). The following inhibitors and ligands were used: TAE684 (NVP-TAE684, Selleckchem, #1108), crizotinib (PR-02341066, Selleckchem #1068), LY 294002 (Tocris), BKM120 (Buparlisib) (Selleckchem, #S2247), AG1024 (Selleckchem #S1234), PPP (CAS 477-47-4, Santa Cruz, scbt #24008), and recombinant murine IGF-1 (Peprotech).

ALKAL2-containing conditioned medium (ACM) was generated as described previously (Guan *et al*, 2015) with slight modifications. Briefly, HEK293T cells, in 10 cm plates, were transfected with 8.0 μg pcDNA3-FAM150B-HA using the calcium phosphate method. After 16 h, media was replaced with starvation medium (DMEM, supplemented with 0.2% FBS, 50 IU/ml penicillin, and 50 μg/ml streptomycin) and ALKAL2-conditioned medium was collected after 36 h. Cortical neurons were treated with CCM and ACM, supplemented with 2% B27 and 1% N2. Activation of wild-type endogenous ALK was confirmed in IMR-32 human neuroblastoma cells.

Protein extraction, immunoblotting, immunoprecipitation, and binding assays

Cultured cells and primary cortical neurons were lysed on ice in lysis buffer (50 mM Tris, pH 7.4, 150 mM NaCl, 1 mM EDTA, and 1% Triton X-100), supplemented with phosphatase and protease inhibitors (Bao *et al*, 2012). Embryonic brains from wild-type or knockout mice were homogenized on ice in lysis buffer, and cleared supernatants were used for immunoblot analysis. For immunoblotting, protein concentrations were determined using the Bradford assay (BioRad) prior to SDS–PAGE. Antibodies used are listed in Appendix Table S2. For co-immunoprecipitation studies, lysates were incubated with the primary antibody at 4°C for 2 h or overnight and then incubated with protein G- or protein A-Sepharose (GE Healthcare) for 2 h. Samples were washed with wash buffer (50 mM Tris, pH 7.4, 150 mM NaCl, 1 mM EDTA, and 0.1% Triton X-100) and were resuspended in SDS-sample buffer. For binding assays, recombinant GST (SignalChem #G52-30U) and GST-LTK (SignalChem #L11-11G) or GST-ALK (SignalChem #A19-116) were incubated with GSH-Sepharose beads (GE Healthcare) in 400 μl binding buffer (50 mM Tris, pH 7.4, 150 mM NaCl, 1 mM EDTA, and 0.5% NP-40) for 1 h at 4°C. Immobilized recombinant proteins were then incubated with 400 μl embryonic brain homogenates or with recombinant His-IGF-1R (SignalChem #I02-11H) for 2 h. Samples were washed three times with binding buffer and were resuspended in SDS-sample buffer.

In vitro kinase assay

Recombinant GST-tagged LTK (SignalChem #L11-11G) was incubated in the absence or in the presence of an equal amount of recombinant His-tagged IGF-1R (SignalChem #I02-11H) in kinase buffer (50 mM HEPES, pH 7.5, 100 mM NaCl, 2 mM DTT, 5 mM $MgCl_2$), supplemented with 150 μM cold ATP and 10 μCi [γ-^{32}P]

© 2023 The Authors

ATP (Perkin Elmer) for 30 min at 30°C. Reactions were terminated with SDS-loading buffer. HEK293T cells were transfected with Flag-tagged IGF-1R alone or together with HA-tagged LTK. Flag immunoprecipitates of IGF-1R-Flag were incubated with Protein G Sepharose beads (GE Healthcare). Beads were pelleted and washed three times in wash buffer and three times in kinase buffer. Kinase reactions were performed for 30 min at 30°C in kinase buffer, supplemented with 150 μM cold ATP and with 10 μCi [γ-^{32}P] ATP (Perkin Elmer). Reactions were stopped by the addition of gel loading buffer and were separated by SDS–PAGE. Gels were dried and the phosphorylation products of kinase reactions were detected by phosphorimaging.

Cell-surface biotinylation assay

High-density cortical neuron cultures or T-REx-LTK cells were cooled on ice to prevent receptor endocytosis and were rinsed with PBS supplemented with 0.5 mM $MgCl_2$ and 1 mM $CaCl_2$. The cell-surface expression level of IGF-1R was examined using membrane-impermeable biotin EZ-Link Sulfo-NHS-LC-biotin (Pierce). Cells were incubated with 1 mg/ml biotin for 20 min on ice and unreacted biotin was removed by three washes with a quenching agent (50 mM glycine and 0.5% BSA in PBS with $MgCl_2$ and $CaCl_2$). Cells were lysed in RIPA buffer containing protease and phosphatase inhibitors and biotinylated proteins were precipitated with NeutrAvidin agarose resin (Pierce). In some experiments, cells were incubated with CCM or ACM on ice or at 37°C to allow endocytosis and then were lysed and precipitated with NeutrAvidin agarose beads. Agarose beads were washed twice in RIPA containing 500 mM NaCl and once in standard RIPA buffer. Biotinylated surface proteins and total lysates were subjected to immunoblotting and quantitated using Image J software (NIH, Bethesda).

RNA extraction and real-time PCR

Total RNA was extracted from primary cortical neurons or brain tissues using Pure Link RNA Mini Kit (Life Technologies) and reverse transcribed into cDNA using oligo dT primers and M-MLV Reverse Transcriptase (Invitrogen). Real-time PCR was performed on Quant Studio 6 Flex Real-time PCR system (Applied Biosystems) using SYBR Green Master mix (Applied Biosystems). Relative gene expression was quantified by $\Delta\Delta C_t$ method and normalized to HPRT1 or GAPDH. The validated primer sequences are listed in Appendix Table S3.

Immunocytochemistry

Neuronal cultures were fixed using 4% (w/v) PFA for 15 min except for cultures used for Tau-1 staining where fixation was performed for 30 min. Fixed cells were permeabilized with 0.2% Triton X-100 in PBS for 5 min, washed with PBS, and blocked at room temperature for 1 h using either 3% bovine serum albumin (BSA, Sigma) or 5% goat serum according to the primary antibody used. Cells were incubated overnight at 4°C with primary antibodies, washed twice with PBS, and incubated with secondary antibodies at room temperature for 1 h. Cells were washed and directly visualized or were fixed and mounted with ProLong Gold (ThermoFisher). Images were taken in a random fashion using a Zeiss inverted microscope equipped with CCD camera (Hamamatsu Photonic Systems) and Volocity software (Perkin Elmer).

Histology and staining of brain sections

Mice were anesthetized with 2.5% Avertin (2,2,2-tribromethanol, Sigma) and perfused transcardially with 4% paraformaldehyde in 0.1 M Na-phosphate buffer, pH 7.4 (PFA). Brains were removed and stored at 4°C overnight in fixative, and then for 1 day at 4°C in 30% sucrose in 0.1 M phosphate buffer, pH 7.4. Brains were cryosectioned using Leica CM3050S cryostat and processed for staining. For Nissl staining, cryosectioned brain slices on slides were immersed in 1:1 alcohol/chloroform at room temperature overnight and then were rehydrated sequentially through 100%, 95% alcohol, and then distilled water. Slides were stained with 0.1% cresyl violet solution for 3–5 min, rinsed quickly in distilled water, developed in 95% ethyl alcohol up to 20 min, dehydrated in 100% alcohol twice for 5 min each, cleared using xylene twice for 5 min each, and then mounted with permanent mounting medium. For immunohistochemistry, brain sections were stained as previously described (Polleux & Ghosh, 2002) using antibodies listed in Appendix Table S3. For quantitation in P2 and P7 mice, cells located within each of eight equally sized bins spanning the cortex were counted and were plotted as a percent of $DAPI^+$ cells. For Golgi staining, brains, from adult mice, at least 3 per genotype, were impregnated with Golgi-Cox solution at room temperature in the dark for 30 days using the FD Rapid Golgi Stain Kit (FD Neurotechnologies). Brains were then transferred to solution C for 2 days, followed by cryosectioning at 60 μm and staining according to the manufacturer's protocol. Pyramidal neurons in layer V of the neocortex and the callosal tract were captured by brightfield microscopy.

In vivo migration assays using BrdU labelling

E14.5 pregnant wild-type, $Alk^{-/-}$, $Ltk^{-/-}$, and *DKO* mice were labeled *in vivo* by intraperitoneal injections with BrdU (150 μg/g body weight, Sigma-Aldrich). In some experiments, PPP (20 mg/kg body weight; Girnita *et al*, 2004) or saline (as control) were injected 24 h after BrdU. E17.5 embryos, P2 and P7 pups were sacrificed and brains were fixed in 4% PFA and cryoprotected in 30% (w/v) sucrose at 4°C overnight. Serial cryosections (12 μm) were incubated with anti-BrdU antibody at 4°C overnight. For quantitation in P2 and P7 mice, $BrdU^+$ cells located within each of eight equally sized bins spanning the cortex were counted.

In situ hybridization

Single-molecule fluorescence *in situ* hybridization (smFISH) was performed using Multiplex Fluorescent Reagent Kit (v2) according to the manufacturer's instructions (Advanced Cell Diagnostics), with probes targeting *Alk* (cat# 501131-C1), *Ltk* (cat# 530801-C2), and *Alkal2* (cat# 531801-C3). Positive (POLR2A: Channel C1, PPIB: Channel C2, UBC: Channel C3: cat#320881) and negative (Bacterial dap gene: cat# 320871) probes were used to validate specificity. Briefly, embryonic (E15-16) or transcardially perfused adult brains were fixed in 4% PFA for 24 h, cryoprotected in 30% (w/v) sucrose for 24 h at 4°C, and coronally cryosectioned at 20 μm. Sections were treated with target retrieval reagent for 5 min, followed by

 © 2023 The Authors

40°C in proteases plus permeabilization for 10 min for embryonic brain and 30 min for adult brain. Sections were immunostained using antibodies listed in Appendix Table S2. Confocal images were acquired using a Nikon Ti2 inverted confocal microscope and analyzed using Volocity software (Perkin Elmer). Widefield images were acquired using Zeiss Axio Scan Z1 and analyzed with Zeiss Zen Black software.

Behavioral studies

Knockout and wild-type animals were tested on a battery of physical and cognitive behavioral studies. Mice were assigned to experimental groups using simple randomization that assured age matching between experimental conditions. *Dark and Light box*. This assay for anxiety-related behavior was carried out as described previously (Holmes *et al*, 2002). The apparatus consisted of a clear plexiglass cage (44 × 21 × 21 cm), illuminated by a 60 W desk lamp overhead and a compartment made from black plexiglass with a covered top. Compartments were separated by a partition, with a small opening (12 × 5 cm) at floor level. Mice were placed in the light compartment, facing away from the partition, and allowed to explore freely for 3 min. The latency to enter the dark box and the number of light–dark transitions (re-enters) and the length of time in light or dark were recorded. *Y-maze test*. Spatial memory was tested in a Y-maze (Miedel *et al*, 2017; Kraeuter *et al*, 2019), consisting of three identical arms with dimensions 38 × 76 × 12.7 cm that met at the center separated by an angle of 120° between each pair of arms (San Diego Instruments). Mice were placed at the end of one arm facing the center and explorations were recorded for 8 min by a camera mounted above the maze and by video-tracking software (Bioserve Viewer2). Entries of all four paws, 5 cm into the arm were recorded. Alternation behavior comprising consecutive entries into each of the three arms without repetition was monitored with the percentage of spontaneous alternations (actual alternation divided by the possible alternations (i.e., total entries-2) × 100) quantitated (Miedel *et al*, 2017). *Puzzle box paradigm*. The Puzzle box assesses cognitive flexibility and problem-solving ability in which mice must leave a brightly lit, open arena to reach a dark, enclosed area through the increasing complexity of barriers as previously described (Ben Abdallah *et al*, 2011). Each Day, three trials were performed with a 2-min inter-trial interval for a maximum of 5 min per trial. On Day 1, trial 1, both the doorway and underpass were open while in trials 2 and 3, only the underpass was open. On Day 2, trial 4, only the underpass is open while in trials 5 and 6 the underpass was blocked with bedding. On Day 3, trial 7, the underpass was blocked with bedding while in trials 8 and 9, the underpass was blocked with a removable cardboard plug.

Statistical analysis

Statistical evaluation between two groups was performed using unpaired Student's *t*-tests and between more than two groups was carried out using one-way ANOVA with the Dunnett's *post hoc* analysis as indicated in the figure legends. The quantitative results are expressed as the mean ± the standard error of the mean (SEM). For all analyses performed, significance was defined as $****P < 0.0001$, $***P < 0.001$, $**P < 0.01$, $*P < 0.05$, and ns, not significant. Data were analyzed using Prism v8 (Graph Pad Software) in a blinded manner.

Data availability

This study includes no data deposited in external repositories.

Expanded View for this article is available online.

Acknowledgements
We thank Dr. Stephen Morris (St. Jude CRH, Memphis) and Dr. Joseph Weiss (OHSU, Oregon) for kindly providing Alk and Ltk knockout mice, Dr. Ruth Palmer (University of Gotenburg, Sweden) for providing plasmids encoding ALKAL1 and ALKAL2, Dr. Igor Stagljar (University of Toronto) for IMR-32 cells, and Dr. Amy J. Ramsey (University of Toronto) for access to equipment for behavioral studies. The authors wish to thank Xin Zhao, Solmaz Alizadeh, and Peter Poliszczuk for technical support during the early stages of the project. This work was funded by a CIHR Foundation grant (#FDN148455) to LA.

Author contributions
Tania Christova: Conceptualization; data curation; formal analysis; investigation; visualization; methodology; writing – original draft; writing – review and editing. **Stephanie KY Ho:** Conceptualization; data curation; formal analysis; investigation; visualization; methodology; writing – original draft; writing – review and editing. **Ying Liu:** Formal analysis; investigation; visualization; methodology. **Mandeep Gill:** Formal analysis; investigation; methodology. **Liliana Attisano:** Conceptualization; resources; supervision; funding acquisition; methodology; writing – original draft; writing – review and editing.

Disclosure and competing interests statement
The authors declare that they have no conflict of interest.

References

Ahmed M, Kaur N, Cheng Q, Shanabrough M, Tretiakov EO, Harkany T, Horvath TL, Schlessinger J (2022) A hypothalamic pathway for Augmentor alpha-controlled body weight regulation. *Proc Natl Acad Sci USA* 119: e2200476119

Arimura N, Kaibuchi K (2007) Neuronal polarity: from extracellular signals to intracellular mechanisms. *Nat Rev Neurosci* 8: 194 – 205

Awad MM, Shaw AT (2014) ALK inhibitors in non-small cell lung cancer: crizotinib and beyond. *Clin Adv Hematol Oncol* 12: 429 – 439

Bao R, Christova T, Song S, Angers S, Yan X, Attisano L (2012) Inhibition of tankyrases induces Axin stabilization and blocks Wnt signalling in breast cancer cells. *PLoS ONE* 7: e48670

Barnes AP, Polleux F (2009) Establishment of axon-dendrite polarity in developing neurons. *Annu Rev Neurosci* 32: 347 – 381

Ben Abdallah NM, Fuss J, Trusel M, Galsworthy MJ, Bobsin K, Colacicco G, Deacon RM, Riva MA, Kellendonk C, Sprengel R *et al* (2011) The puzzle box as a simple and efficient behavioral test for exploring impairments of general cognition and executive functions in mouse models of schizophrenia. *Exp Neurol* 227: 42 – 52

Bilsland JG, Wheeldon A, Mead A, Znamenskiy P, Almond S, Waters KA, Thakur M, Beaumont V, Bonnert TP, Heavens R *et al* (2008) Behavioral and neurochemical alterations in mice deficient in anaplastic lymphoma

© 2023 The Authors

kinase suggest therapeutic potential for psychiatric indications. *Neuropsychopharmacology* 33: 685 – 700

Borenas M, Umapathy G, Lai WY, Lind DE, Witek B, Guan J, Mendoza-Garcia P, Masudi T, Claeys A, Chuang TP *et al* (2021) ALK ligand ALKAL2 potentiates MYCN-driven neuroblastoma in the absence of ALK mutation. *EMBO J* 40: e105784

Bourin M, Hascoet M (2003) The mouse light/dark box test. *Eur J Pharmacol* 463: 55 – 65

Bradke F, Dotti CG (2000) Establishment of neuronal polarity: lessons from cultured hippocampal neurons. *Curr Opin Neurobiol* 10: 574 – 581

Centonze FG, Reiterer V, Nalbach K, Saito K, Pawlowski K, Behrends C, Farhan H (2019) LTK is an ER-resident receptor tyrosine kinase that regulates secretion. *J Cell Biol* 218: 2470 – 2480

Chen G, Sima J, Jin M, Wang KY, Xue XJ, Zheng W, Ding YQ, Yuan XB (2008) Semaphorin-3A guides radial migration of cortical neurons during development. *Nat Neurosci* 11: 36 – 44

Cheng LY, Bailey AP, Leevers SJ, Ragan TJ, Driscoll PC, Gould AP (2011) Anaplastic lymphoma kinase spares organ growth during nutrient restriction in *Drosophila*. *Cell* 146: 435 – 447

Chuang JC, Neal JW (2015) Crizotinib as first line therapy for advanced ALK-positive non-small cell lung cancers. *Transl Lung Cancer Res* 4: 639 – 641

De Munck S, Provost M, Kurikawa M, Omori I, Mukohyama J, Felix J, Bloch Y, Abdel-Wahab O, Bazan JF, Yoshimi A *et al* (2021) Structural basis of cytokine-mediated activation of ALK family receptors. *Nature* 600: 143 – 147

Defaye M, Iftinca MC, Gadotti VM, Basso L, Abdullah NS, Cumenal M, Agosti F, Hassan A, Flynn R, Martin J *et al* (2022) The neuronal tyrosine kinase receptor ligand ALKAL2 mediates persistent pain. *J Clin Invest* 132: e154317

Edwards TJ, Sherr EH, Barkovich AJ, Richards LJ (2014) Clinical, genetic and imaging findings identify new causes for corpus callosum development syndromes. *Brain* 137: 1579 – 1613

Fadeev A, Mendoza-Garcia P, Irion U, Guan J, Pfeifer K, Wiessner S, Serluca F, Singh AP, Nusslein-Volhard C, Palmer RH (2018) ALKALs are in vivo ligands for ALK family receptor tyrosine kinases in the neural crest and derived cells. *Proc Natl Acad Sci USA* 115: E630 – E638

Fernandez AM, Torres-Aleman I (2012) The many faces of insulin-like peptide signalling in the brain. *Nat Rev Neurosci* 13: 225 – 239

Galetta D, Rossi A, Pisconti S, Colucci G (2012) The emerging role of ALK inhibitors in the treatment of advanced non-small cell lung cancer. *Expert Opin Ther Targets* 16: S45 – S54

Girnita A, Girnita L, del Prete F, Bartolazzi A, Larsson O, Axelson M (2004) Cyclolignans as inhibitors of the insulin-like growth factor-1 receptor and malignant cell growth. *Cancer Res* 64: 236 – 242

Gotz M, Huttner WB (2005) The cell biology of neurogenesis. *Nat Rev Mol Cell Biol* 6: 777 – 788

Gouzi JY, Moressis A, Walker JA, Apostolopoulou AA, Palmer RH, Bernards A, Skoulakis EM (2011) The receptor tyrosine kinase Alk controls neurofibromin functions in *Drosophila* growth and learning. *PLoS Genet* 7: e1002281

Guan J, Umapathy G, Yamazaki Y, Wolfstetter G, Mendoza P, Pfeifer K, Mohammed A, Hugosson F, Zhang H, Hsu AW *et al* (2015) FAM150A and FAM150B are activating ligands for anaplastic lymphoma kinase. *Elife* 4: e09811

Hallberg B, Palmer RH (2016) The role of the ALK receptor in cancer biology. *Ann Oncol* 27: iii4 – iii15

Holmes A, Yang RJ, Crawley JN (2002) Evaluation of an anxiety-related phenotype in galanin overexpressing transgenic mice. *J Mol Neurosci* 18: 151 – 165

Iwahara T, Fujimoto J, Wen D, Cupples R, Bucay N, Arakawa T, Mori S, Ratzkin B, Yamamoto T (1997) Molecular characterization of ALK, a receptor tyrosine kinase expressed specifically in the nervous system. *Oncogene* 14: 439 – 449

Izumi H, Matsumoto S, Liu J, Tanaka K, Mori S, Hayashi K, Kumagai S, Shibata Y, Hayashida T, Watanabe K *et al* (2021) The CLIP1-LTK fusion is an oncogenic driver in non-small-cell lung cancer. *Nature* 600: 319 – 323

Janoueix-Lerosey I, Lequin D, Brugieres L, Ribeiro A, de Pontual L, Combaret V, Raynal V, Puisieux A, Schleiermacher G, Pierron G *et al* (2008) Somatic and germline activating mutations of the ALK kinase receptor in neuroblastoma. *Nature* 455: 967 – 970

Janoueix-Lerosey I, Lopez-Delisle L, Delattre O, Rohrer H (2018) The ALK receptor in sympathetic neuron development and neuroblastoma. *Cell Tissue Res* 372: 325 – 337

Jiang H, Guo W, Liang X, Rao Y (2005) Both the establishment and the maintenance of neuronal polarity require active mechanisms: critical roles of GSK-3beta and its upstream regulators. *Cell* 120: 123 – 135

Kraeuter AK, Guest PC, Sarnyai Z (2019) The Y-maze for assessment of spatial working and reference memory in mice. *Methods Mol Biol* 1916: 105 – 111

Lasek AW, Lim J, Kliethermes CL, Berger KH, Joslyn G, Brush G, Xue L, Robertson M, Moore MS, Vranizan K *et al* (2011) An evolutionary conserved role for anaplastic lymphoma kinase in behavioral responses to ethanol. *PLoS ONE* 6: e22636

Laurino L, Wang XX, de la Houssaye BA, Sosa L, Dupraz S, Caceres A, Pfenninger KH, Quiroga S (2005) PI3K activation by IGF-1 is essential for the regulation of membrane expansion at the nerve growth cone. *J Cell Sci* 118: 3653 – 3662

Lewis TL Jr, Courchet J, Polleux F (2013) Cell biology in neuroscience: cellular and molecular mechanisms underlying axon formation, growth, and branching. *J Cell Biol* 202: 837 – 848

Li T, Stayrook SE, Tsutsui Y, Zhang J, Wang Y, Li H, Proffitt A, Krimmer SG, Ahmed M, Belliveau O *et al* (2021) Structural basis for ligand reception by anaplastic lymphoma kinase. *Nature* 600: 148 – 152

Lopes SS, Yang X, Muller J, Carney TJ, McAdow AR, Rauch GJ, Jacoby AS, Hurst LD, Delfino-Machin M, Haffter P *et al* (2008) Leukocyte tyrosine kinase functions in pigment cell development. *PLoS Genet* 4: e1000026

Lovly CM, McDonald NT, Chen H, Ortiz-Cuaran S, Heukamp LC, Yan Y, Florin A, Ozretic L, Lim D, Wang L *et al* (2014) Rationale for co-targeting IGF-1R and ALK in ALK fusion-positive lung cancer. *Nat Med* 20: 1027 – 1034

Maira SM, Pecchi S, Huang A, Burger M, Knapp M, Sterker D, Schnell C, Guthy D, Nagel T, Wiesmann M *et al* (2012) Identification and characterization of NVP-BKM120, an orally available pan-class I PI3-kinase inhibitor. *Mol Cancer Ther* 11: 317 – 328

Mazzeschi M, Sgarzi M, Romaniello D, Gelfo V, Cavallo C, Ambrosi F, Morselli A, Miano C, Laprovitera N, Girone C *et al* (2022) The autocrine loop of ALK receptor and ALKAL2 ligand is an actionable target in consensus molecular subtype 1 colon cancer. *J Exp Clin Cancer Res* 41: 113

Miedel CJ, Patton JM, Miedel AN, Miedel ES, Levenson JM (2017) Assessment of spontaneous alternation, novel object recognition and limb clasping in transgenic mouse models of amyloid-beta and tau neuropathology. *J Vis Exp* 55523

Mo ES, Cheng Q, Reshetnyak AV, Schlessinger J, Nicoli S (2017) Alk and Ltk ligands are essential for iridophore development in zebrafish mediated by the receptor tyrosine kinase Ltk. *Proc Natl Acad Sci USA* 114: 12027 – 12032

Molyneaux BJ, Arlotta P, Menezes JR, Macklis JD (2007) Neuronal subtype specification in the cerebral cortex. *Nat Rev Neurosci* 8: 427 – 437

 © 2023 The Authors

Morris SW, Kirstein MN, Valentine MB, Dittmer K, Shapiro DN, Look AT, Saltman DL (1995) Fusion of a kinase gene, ALK, to a nucleolar protein gene, NPM, in non-Hodgkin's lymphoma. *Science* 267: 316 – 317

Muller-Tidow C, Schwable J, Steffen B, Tidow N, Brandt B, Becker K, Schulze-Bahr E, Halfter H, Vogt U, Metzger R *et al* (2004) High-throughput analysis of genome-wide receptor tyrosine kinase expression in human cancers identifies potential novel drug targets. *Clin Cancer Res* 10: 1241 – 1249

Nieto Guil AF, Oksdath M, Weiss LA, Grassi DJ, Sosa LJ, Nieto M, Quiroga S (2017) IGF-1 receptor regulates dynamic changes in neuronal polarity during cerebral cortical migration. *Sci Rep* 7: 7703

Noctor SC, Flint AC, Weissman TA, Dammerman RS, Kriegstein AR (2001) Neurons derived from radial glial cells establish radial units in neocortex. *Nature* 409: 714 – 720

O'Kusky J, Ye P (2012) Neurodevelopmental effects of insulin-like growth factor signaling. *Front Neuroendocrinol* 33: 230 – 251

Orthofer M, Valsesia A, Magi R, Wang QP, Kaczanowska J, Kozieradzki I, Leopoldi A, Cikes D, Zopf LM, Tretiakov EO *et al* (2020) Identification of ALK in thinness. *Cell* 181: 1246 – 1262

Palmer RH, Vernersson E, Grabbe C, Hallberg B (2009) Anaplastic lymphoma kinase: signalling in development and disease. *Biochem J* 420: 345 – 361

Park J, Choi H, Kim YD, Kim SH, Kim Y, Gwon Y, Lee DY, Park SH, Heo WD, Jung YK (2021) Aberrant role of ALK in tau proteinopathy through autophagosomal dysregulation. *Mol Psychiatry* 26: 5542 – 5556

Parrizas M, Gazit A, Levitzki A, Wertheimer E, LeRoith D (1997) Specific inhibition of insulin-like growth factor-1 and insulin receptor tyrosine kinase activity and biological function by tyrphostins. *Endocrinology* 138: 1427 – 1433

Polleux F, Ghosh A (2002) The slice overlay assay: a versatile tool to study the influence of extracellular signals on neuronal development. *Sci STKE* 2002: pl9

Quiroga S, Bisbal M, Caceres A (2018) Regulation of plasma membrane expansion during axon formation. *Dev Neurobiol* 78: 170 – 180

Reshetnyak AV, Murray PB, Shi X, Mo ES, Mohanty J, Tome F, Bai H, Gunel M, Lax I, Schlessinger J (2015) Augmentor alpha and beta (FAM150) are ligands of the receptor tyrosine kinases ALK and LTK: hierarchy and specificity of ligand-receptor interactions. *Proc Natl Acad Sci USA* 112: 15862 – 15867

Reshetnyak AV, Rossi P, Myasnikov AG, Sowaileh M, Mohanty J, Nourse A, Miller DJ, Lax I, Schlessinger J, Kalodimos CG (2021) Mechanism for the activation of the anaplastic lymphoma kinase receptor. *Nature* 600: 153 – 157

Rieger L, O'Connor R (2020) Controlled signaling-insulin-like growth factor receptor endocytosis and presence at intracellular compartments. *Front Endocrinol (Lausanne)* 11: 620013

Rieger L, O'Shea S, Godsmark G, Stanicka J, Kelly G, O'Connor R (2020) IGF-1 receptor activity in the Golgi of migratory cancer cells depends on adhesion-dependent phosphorylation of Tyr(1250) and Tyr(1251). *Sci Signal* 13: eaba3176

Rodig SJ, Shapiro GI (2010) Crizotinib, a small-molecule dual inhibitor of the c-met and ALK receptor tyrosine kinases. *Curr Opin Investig Drugs* 11: 1477 – 1490

Romero DM, Bahi-Buisson N, Francis F (2018) Genetics and mechanisms leading to human cortical malformations. *Semin Cell Dev Biol* 76: 33 – 75

Roskoski R Jr (2013) Anaplastic lymphoma kinase (ALK): structure, oncogenic activation, and pharmacological inhibition. *Pharmacol Res* 68: 68 – 94

Shiota M, Fujimoto J, Semba T, Satoh H, Yamamoto T, Mori S (1994) Hyperphosphorylation of a novel 80 kDa protein-tyrosine kinase similar to Ltk in a human Ki-1 lymphoma cell line, AMS3. *Oncogene* 9: 1567 – 1574

Solomon BJ, Besse B, Bauer TM, Felip E, Soo RA, Camidge DR, Chiari R, Bearz A, Lin CC, Gadgeel SM *et al* (2018) Lorlatinib in patients with ALK-positive non-small-cell lung cancer: results from a global phase 2 study. *Lancet Oncol* 19: 1654 – 1667

Sosa L, Dupraz S, Laurino L, Bollati F, Bisbal M, Caceres A, Pfenninger KH, Quiroga S (2006) IGF-1 receptor is essential for the establishment of hippocampal neuronal polarity. *Nat Neurosci* 9: 993 – 995

Takano T, Xu C, Funahashi Y, Namba T, Kaibuchi K (2015) Neuronal polarization. *Development* 142: 2088 – 2093

Uhlen M, Fagerberg L, Hallstrom BM, Lindskog C, Oksvold P, Mardinoglu A, Sivertsson A, Kampf C, Sjostedt E, Asplund A *et al* (2015) Proteomics. Tissue-based map of the human proteome. *Science* 347: 1260419

Uzquiano A, Gladwyn-Ng I, Nguyen L, Reiner O, Gotz M, Matsuzaki F, Francis F (2018) Cortical progenitor biology: key features mediating proliferation versus differentiation. *J Neurochem* 146: 500 – 525

Vasilcanu D, Girnita A, Girnita L, Vasilcanu R, Axelson M, Larsson O (2004) The cyclolignan PPP induces activation loop-specific inhibition of tyrosine phosphorylation of the insulin-like growth factor-1 receptor. Link to the phosphatidyl inositol-3 kinase/Akt apoptotic pathway. *Oncogene* 23: 7854 – 7862

Vivancos Stalin L, Gualandi M, Schulte JH, Renella R, Shakhova O, Muhlethaler-Mottet A (2019) Expression of the Neuroblastoma-associated ALK-F1174L activating mutation during embryogenesis impairs the differentiation of neural crest progenitors in sympathetic ganglia. *Front Oncol* 9: 275

Weiss JB, Xue C, Benice T, Xue L, Morris SW, Raber J (2012) Anaplastic lymphoma kinase and leukocyte tyrosine kinase: functions and genetic interactions in learning, memory and adult neurogenesis. *Pharmacol Biochem Behav* 100: 566 – 574

Witek B, El Wakil A, Nord C, Ahlgren U, Eriksson M, Vernersson-Lindahl E, Helland A, Alexeyev OA, Hallberg B, Palmer RH (2015) Targeted disruption of ALK reveals a potential role in hypogonadotropic hypogonadism. *PLoS ONE* 10: e0123542

Xu Q, Cobos I, De La Cruz E, Rubenstein JL, Anderson SA (2004) Origins of cortical interneuron subtypes. *J Neurosci* 24: 2612 – 2622

Yao S, Cheng M, Zhang Q, Wasik M, Kelsh R, Winkler C (2013) Anaplastic lymphoma kinase is required for neurogenesis in the developing central nervous system of zebrafish. *PLoS ONE* 8: e63757

Yoshimura T, Arimura N, Kawano Y, Kawabata S, Wang S, Kaibuchi K (2006) Ras regulates neuronal polarity via the PI3-kinase/Akt/GSK-3beta/CRMP-2 pathway. *Biochem Biophys Res Commun* 340: 62 – 68

Zhang H, Pao LI, Zhou A, Brace AD, Halenbeck R, Hsu AW, Bray TL, Hestir K, Bosch E, Lee E *et al* (2014) Deorphanization of the human leukocyte tyrosine kinase (LTK) receptor by a signaling screen of the extracellular proteome. *Proc Natl Acad Sci USA* 111: 15741 – 15745

Zhou Z, He G, Zhang X, Lv X, Zhang X, Liu A, Xia S, Xie H, Dang R, Han L *et al* (2021) NGPF2 triggers synaptic scaling up through ALK-LIMK-cofilin-mediated mechanisms. *Cell Rep* 36: 109515

License: This is an open access article under the terms of the Creative Commons Attribution-NonCommercial-NoDerivs License, which permits use and distribution in any medium, provided the original work is properly cited, the use is non-commercial and no modifications or adaptations are made.

Expanded View Figures

Figure EV1. Expression of Ltk, Alk, and Alkal2 in murine embryonic and adult cortex and brain.

A Expression of Alk, Ltk, and Alkal2 at E15.5 was determined by single-molecule *in situ* analysis. A representative coronal widefield DAPI stained image (blue) of a coronal section of an E15.5 brain (left). Higher magnifications of the inset region (right panels) show mRNA expression of Ltk (green), Alk (yellow), and the ligand, Alkal2 (red), and are counterstained with Sox2 protein (anti-Sox2: purple) and DAPI (blue). Dashed lines mark the upper limit of the SVZ. Scale bars are 100 μm.

B A high magnification (63×) image from the SVZ shows mRNA expression of Alk (green), Ltk (yellow), and Alkal2 (red) counterstained with DAPI (blue). Scale bars are 20 μm.

C–F Ltk and Alk are expressed in distinct patterns in E15.5 embryos during the onset of neurogenesis and cortical plate formation. (C) Schematic denoting the approximate location of coronal sections E15.5 at which the expression was examined in (D–F) rostral to caudal, respectively. (D–F) Ltk (yellow) is found rostrally in the neo-cortical plate (CP), claustrum (Cl), accumbens nucleus (AC), amygdaloid area (AAA), and caudate putamen (cp). High expression of Ltk was observed in thalamic area, ventral thalamic nucleus (vl), paraventricular thalamic nucleus (pvt), hypothalamic area (ah), and globus pallidus (gp). Alk (green) was prominently expressed near ventricular regions throughout the neocerebrum with robust expression in the area of the medial spectrum nucleus (ms), lateral olfactory bulb (Lot), paraventricular thalamic nucleus (pvt), ventromedial thalamic nucleus (Vmt), pretactal area (Pre), and subcommissural organ (Sco). Alka2 (red), is expressed in many regions, overlapping with Ltk and Alk. Co-expression was observed throughout the cortical plate (CP), ventricular zone (Vz), ventrolateral thalamic nucleus (vl), lateral olfactory bulb (Lot), amygdaloid area (AAA), and hypothalamic area (ah). Bma, basomedial amygdala; cmt, centromedium thalamic nucleus; de, dorsal endopyriform nucleus; Hi, hippocampus; mfb, medial forebrain bundle; pf, plexiform; Ph, posterior hypothalamic area; and Vpm, ventral premammilary nucleus. Scale bars are 100 μm.

G The expression levels of Alk, Ltk, and Alkal2 mRNA in the embryonic, postnatal (P2 and P7) and adult (3–6 month) cortex, and brain were determined by qPCR.

Data information: Data are plotted as the mean ± SEM, from three independent biological experiments.

© 2023 The Authors

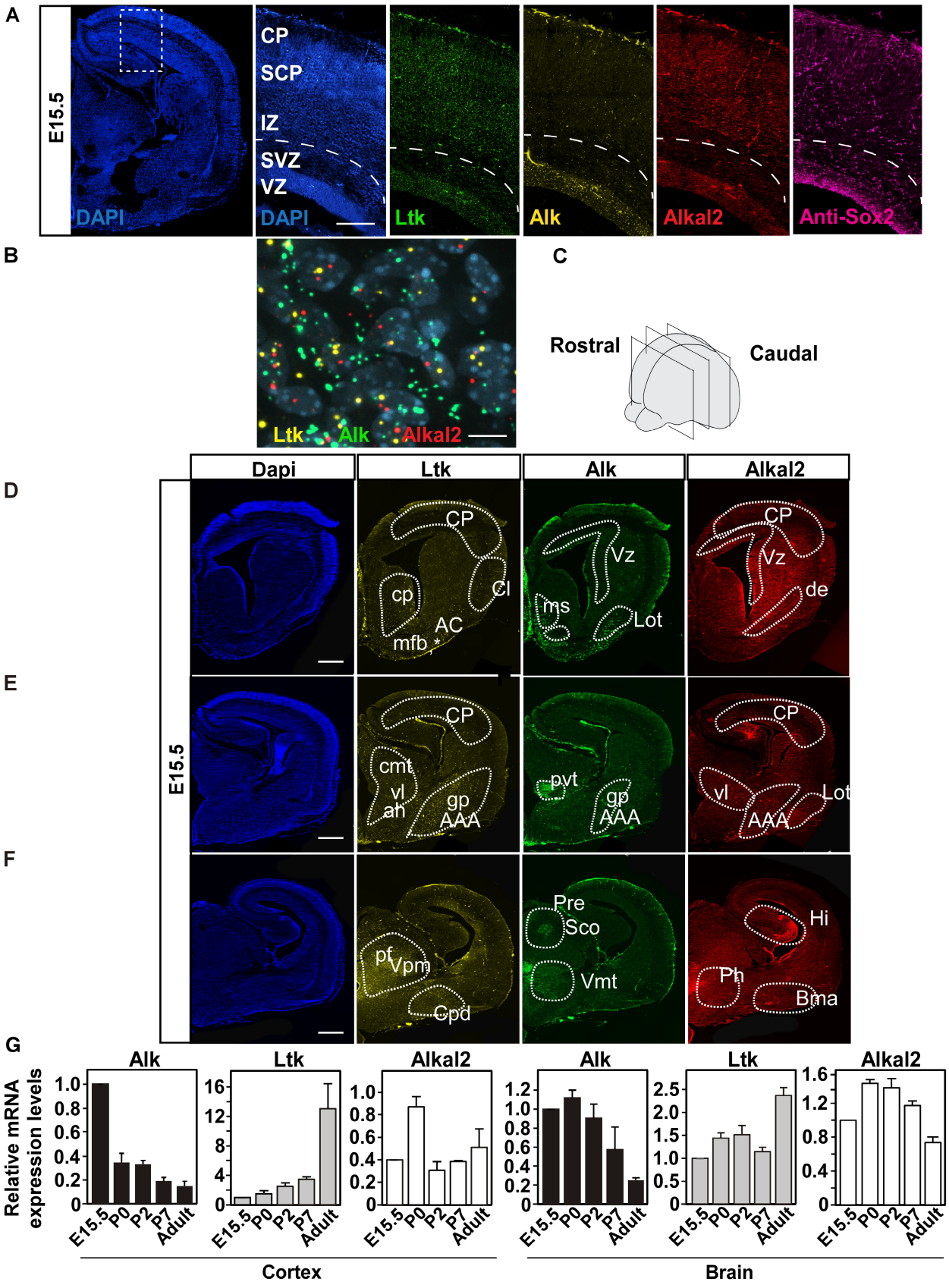

A
E15.5
DAPI
CP
SCP
IZ
SVZ
VZ
DAPI
Ltk
Alk
Alkal2
Anti-Sox2
B
Ltk
Alk
Alkal2
C
Rostral
Caudal
D
E
F
Dapi
Ltk
Alk
Alkal2
E15.5
CP
cp
Cl
AC
mfb
Vz
ms
Lot
de
cmt
vl
ah
gp
AAA
pvt
Pre
Sco
Vmt
pf
Vpm
Cpd
Hi
Ph
Bma
G
Relative mRNA expression levels
Alk
Ltk
Alkal2
E15.5
P0
P2
P7
Adult
Cortex
Brain

Figure EV1.

Figure EV2. Disruption of Ltk and Alk alters early cortical plate patterning.

A, B Coronal sections of E15.5 WT, $Ltk^{-/-}$ and $Alk^{-/-}$ developing cortices were co-stained with either anti-Sox2 (green) and anti-Pax6 (red) or with anti-Sox2 (green) and anti-Tbr2 (red) and both counterstained with DAPI (blue). Scale bars are 50 μm. Quantitation of total $DAPI^+$ cells and $Sox2^+$, $Pax6^+$, or $Tbr2^+$ progenitor cells in the SVZ/VZ in the entire image, corresponding to an area of 100 × 100 μM are plotted.

C–F Coronal sections of WT, $Ltk^{-/-}$ and $Alk^{-/-}$ developing cortices stained with DAPI (blue) and co-stained with anti-Ctip2 (red) and Satb2 (green) at P2 and P7. The location of the cortical plate (CP), intermediate zone (IZ), subventricular/ventricular zone (SVZ/VZ) in P2 mice, and Layers I-VI in P7 WT mice is indicated. Scale bars are 50 μm. (D, F) Quantitation of $Ctip2^+$ and $Satb2^+$ progenitor cells as a percent of total $DAPI^+$ cells in each of 8 bins (marked on left) within the cortex (dashed lines) in a total area corresponding to 100 × 600 μM are plotted.

Data information: Data in (B, D, F) are presented as the mean ± SEM of three independent biological experiments. Statistical significance: $^{**}P < 0.01$, $^{*}P < 0.05$ by one-way ANOVA using the Dunnett's test.

© 2023 The Authors

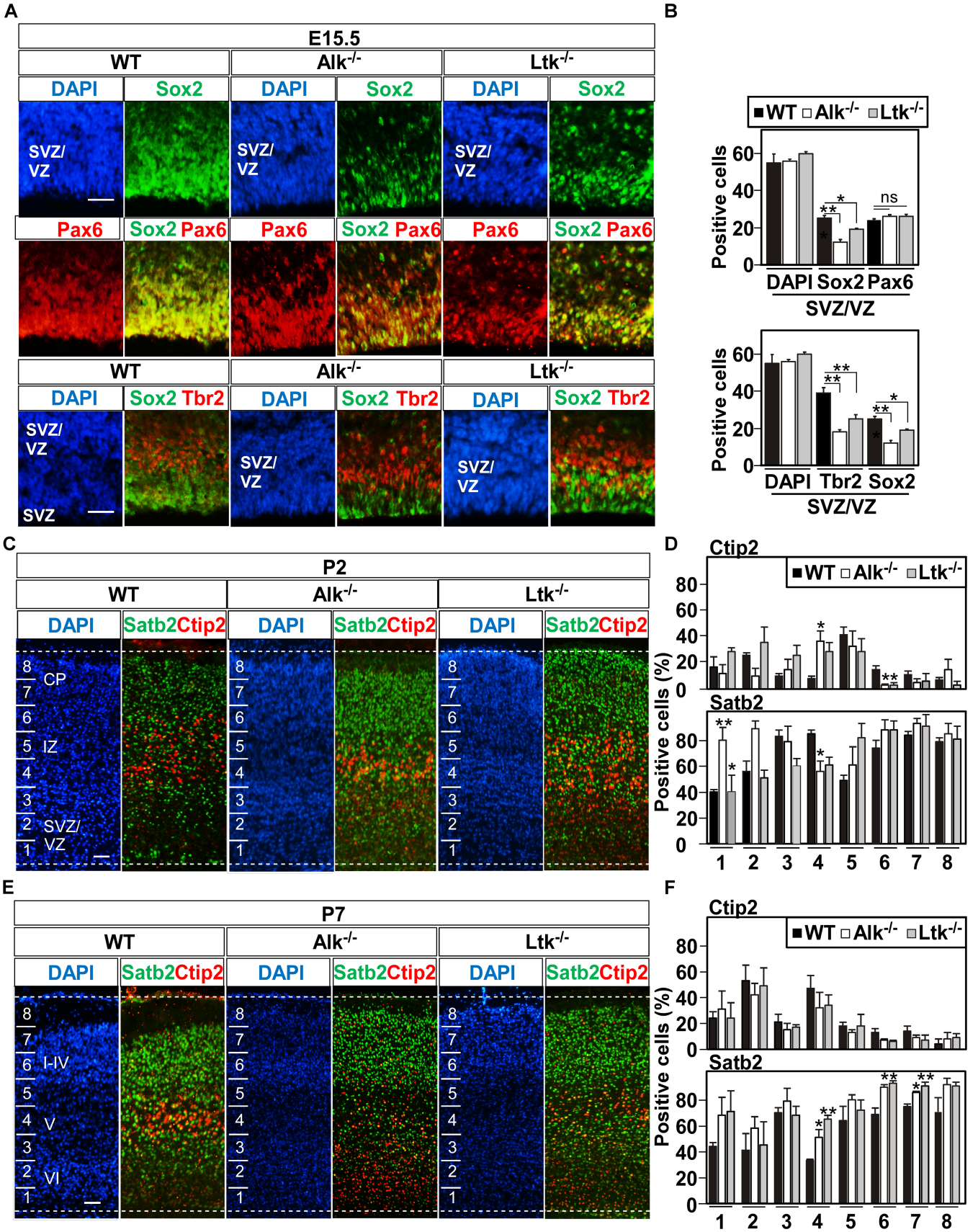

A
E15.5
WT
Alk-/-
Ltk-/-
DAPI
Sox2
SVZ/
VZ
Pax6
Sox2 Pax6
Sox2 Tbr2
SVZ
B
WT Alk-/- Ltk-/-
Positive cells
DAPI Sox2 Pax6
SVZ/VZ
DAPI Tbr2 Sox2
ns
C
P2
Satb2Ctip2
CP
IZ
SVZ/
VZ
D
Ctip2
Satb2
Positive cells (%)
E
P7
I-IV
V
VI
F

Figure EV2.

Figure EV3. ALKAL2 ligand-mediated activation of LTK/ALK results in defects in neuronal polarity. PI3 kinase is activated in cortical neurons from knockout mice.

A The expression of Alkal2 mRNA in E16 dissociated cortical neurons or in embryonic, P20, and adult (3–6 month) brain in WT and DKO mice was determined by qPCR.
B Alkal2 knockdown efficiency was determined by real-time PCR.
C IMR-32 cells were treated for 20 min with control (CCM) or ALKAL2 (ACM)-conditioned media. Representative immunoblots indicating the levels of pALK (pALK^{Y1586}), pAKT (pAKT^{S473}), and total ALK and AKT in cell lysates are shown. The increased levels of phosphorylated ALK and AKT indicate that ligand addition increased the activity of ALK and ALK downstream signaling.
D Treatment of cortical neurons from WT or KO mice with PI3 kinase inhibitors reverses polarity defects caused by loss of Ltk/Alk. Dissociated E16 cortical neurons were treated with LY294002 (10 μM) or DMSO control, 4 h after plating and then fixed at 33 h and stained with phalloidin. Arrowheads mark the axon-like projections. Scale bars are 20 μm.
E Inhibition of PI3K reverses the effect of siRNA-mediated knockdown of Ltk/Alk in cortical neurons. Representative images of dissociated E16 WT cortical neurons co-transfected with the indicated siRNAs and GFP were treated with LY294002 (PI3K inhibitor) 6 h after plating and then fixed at 33 h. Arrowheads mark the axon-like projections. Scale bars are 20 μm.
F Ectopic expression of PTEN rescues the multiple axon phenotype in cortical neurons. Representative images of cortical neurons, isolated from WT or DKO embryos and transfected with plasmids encoding GFP alone or HA-tagged PTEN. Arrowheads mark the axon-like projections. Scale bars are 20 μm.
G Analysis of brain homogenates reveals activated downstream PI3 kinase signaling in DKO mice. Brain lysates from individual mice of the indicated genotypes were subjected to immunoblotting with antibodies against phosphorylated AKT (pAKT^{S473}) and AKT. Blots were re-probed with GAPDH antibody as a loading control. Quantitation of band intensities for pAkt to Akt in each lane and the fold change relative to control WT1 (WT, mouse #1, marked by a red line) is plotted.

Data information: Data in (A, B) are plotted as the mean ± SD from three independent biological experiments. Quantitation of neurons with multiple, single or no axon-like projections in (D–F) is plotted as the mean ± SD, (n = 100 neurons per condition) from three independent biological experiments. Data in (D, E) were analyzed using one-way ANOVA and comparisons with the concurrent DMSO control were performed using the Dunnett's test. Data in (B, F**)** were analyzed using a two-tailed Student's t-test. Statistical significance: ****$P < 0.0001$, ***$P < 0.001$, **$P < 0.01$, *$P < 0.05$.
Source data are available online for this figure.

© 2023 The Authors

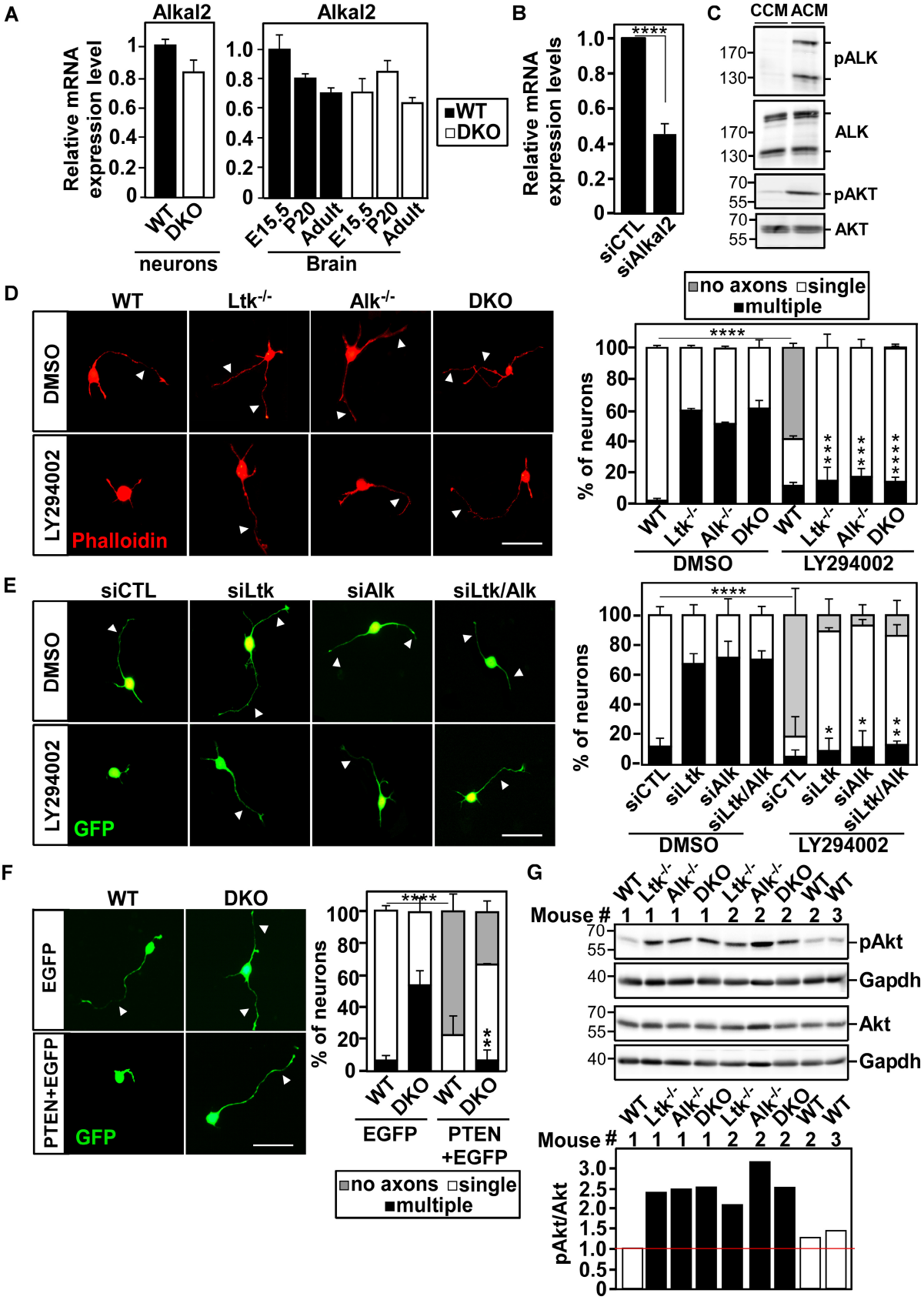

A
Alkal2
Relative mRNA expression level
WT
DKO
neurons
E15.5
P20
Adult
Brain
B
Relative mRNA expression levels
siCTL
siAlkal2
C
CCM ACM
pALK
ALK
pAKT
AKT
D
WT
Ltk-/-
Alk-/-
DKO
DMSO
LY294002
Phalloidin
no axons single multiple
% of neurons
E
siCTL
siLtk
siAlk
siLtk/Alk
GFP
F
EGFP
PTEN+EGFP
PTEN +EGFP
G
Mouse #
pAkt
Gapdh
Akt
pAkt/Akt

Figure EV3.

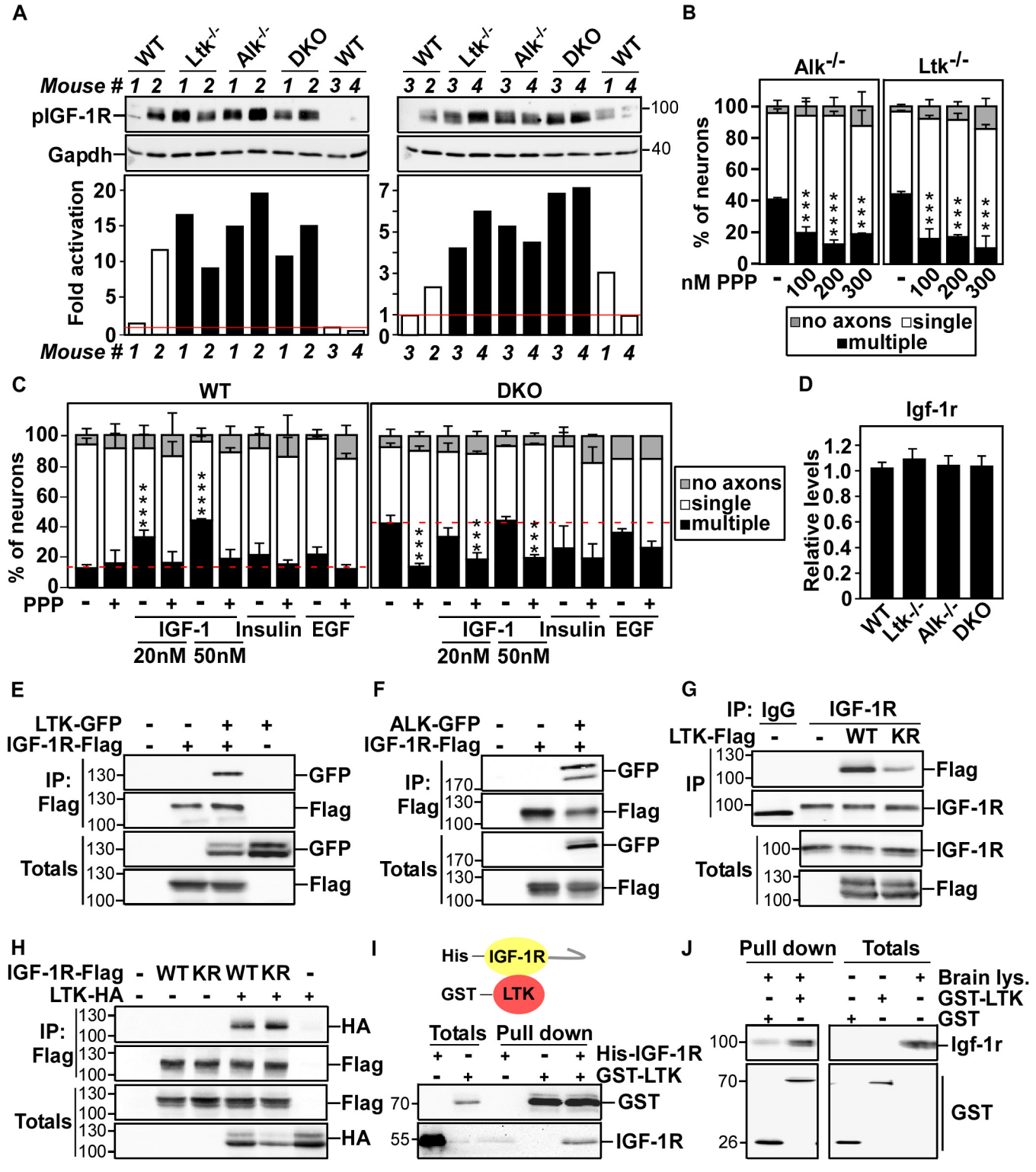


Figure EV4.

© 2023 The Authors

Figure EV4. LTK/ALK interacts with IGF-1R and modulates its activity. Loss of LTK/ALK promotes IGF-1R activity.

A Lysates from cortical neurons from four individual mice of the indicated genotypes were subjected to immunoblotting with phospho-IGF-1R (pIGF-1R$^{Y1135/1136}$) and Gapdh as a control to verify equal protein loading. Quantitation of band intensities for pIGF-1R/Gapdh as fold change relative to control WT3 (WT, mouse #3, marked by a red line) is plotted.

B The IGF-1R inhibitor, PPP rescues the multiple axon phenotype in cortical neurons from Alk or Ltk knockout mice. Cortical neurons, isolated from Alk or Ltk knockout mice were treated with varying concentrations of PPP or DMSO as control 4 h after plating, fixed, and stained for Tuj1. Quantitation of the percent of neurons with multiple, single or no axon-like projections is plotted.

C Analysis of the effect of ectopically applied recombinant IGF-1. Cortical neurons isolated from WT or DKO mice electroporated with a GFP plasmid were treated with PPP (200 nM), DMSO as control and /or IGF-1 (20 or 50 nM), insulin (100 nM) or EGF (20 ng/ml). Cells were fixed at 33 h and GFP-positive cells were analyzed. Quantitation of the percent of neurons with multiple, single or no axon-like projections is plotted.

D Expression of Igf-1r mRNA was determined by qPCR in cortical neurons from WT and knockout mice.

E, F IGF-1R associates with LTK and ALK in HEK293T cells. Lysates from HEK 293T cells, transfected with IGF-1R-Flag, LTK-GFP (E), or ALK-GFP (F) were subjected to immunoprecipitation using anti-Flag antibody and co-precipitated LTK (E) or ALK (F) was detected by immunoblotting using anti-GFP antibody.

G LTK activity is required for interaction with IGF-1R. HEK293T cells were transfected with wild-type (WT) or kinase-inactive (KR) versions of LTK-Flag. Endogenous IGF-1R was immunoprecipitated with anti-IGF-1R antibody and co-precipitated LTK-Flag was detected by immunoblotting with anti-Flag antibody.

H LTK/ALK interacts with WT and kinase-inactive (KR) variants of IGF-1R. Lysates from HEK293T cells, co-transfected with LTK-WT-HA and WT or KR versions of IGF-1R-Flag were subjected to immunoprecipitation with anti-Flag antibody and co-precipitated LTK was detected by immunoblotting with anti-HA antibody.

I GST-LTK immobilized to GSH-Sepharose beads was incubated with recombinant His-IGF-1R. Pulldowns and totals were subjected to immunoblotting using the indicated antibodies.

J Purified recombinant GST-LTK interacts with endogenous Igf-1r. Lysates from WT embryonic brains were incubated with GST-LTK or GST alone and immobilized to GSH-Sepharose beads. Bound and total proteins were subjected to immunoblotting with anti-IGF-1R antibody.

Data information: Data in (B, D) are plotted as the mean ± SD of three independent biological experiments. Data in (C) are plotted as the mean ± SD, $n = 100$ neurons from 2 (for EGF) or $n = 200$ neurons from 4 (remainder) independent biological experiments. A representative result from three independent biological experiments is shown in (E–J). Data in (B, C) were analyzed using one-way ANOVA, and comparisons with control were performed using the Dunnett's test (****$P < 0.0001$, ***$P < 0.001$).
Source data are available online for this figure.

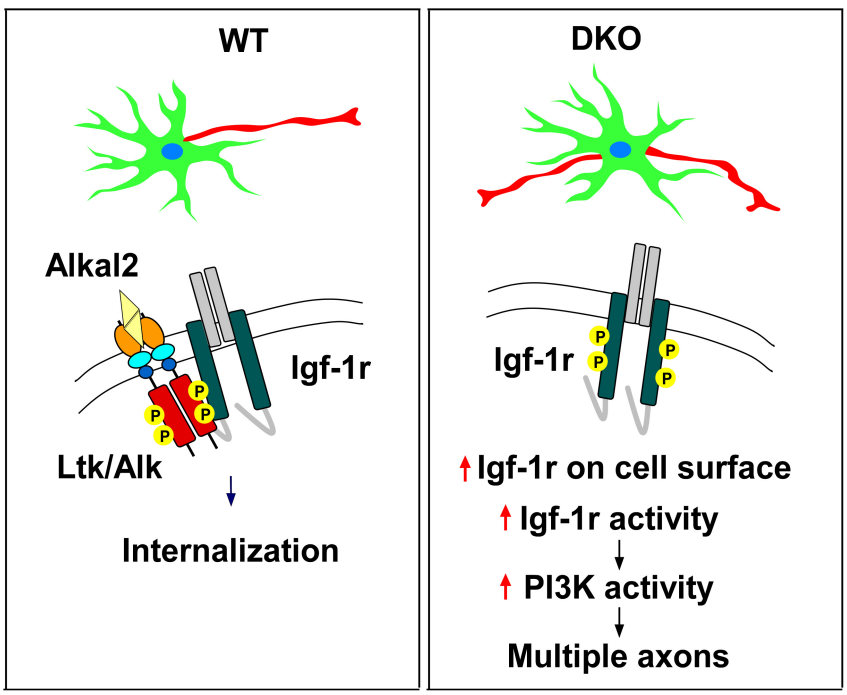


Figure EV5. A model depicting the role of Ltk and Alk in regulating neuronal morphology through modulation of Igf-1r activity.

In WT neurons, ligand-induced activation of Ltk/Alk favors interaction with and internalization of Igf-1r. This reduces cell-surface expression of Igf-1r and maintains proper neuronal morphology. Loss of Alk and Ltk increases the cell-surface expression and activity of Igf-1r, that in turn, activates downstream PI3 kinase signaling to drive the multiple axon phenotype.

© 2023 The Authors

APPENDIX

LTK and ALK promote neuronal polarity and cortical migration by modulating IGF1R activity

Tania Christova, Stephanie Ho, Ying Liu, Mandeep Gill, and Liliana Attisano

Table of content

Appendix Figure S1: Analysis of coronal sections of WT and Ltk/Alk knockout mice by Nissl and Golgi staining…… Page 1

Appendix Figure S2: Ctip2 and Satb2 positive cells in WT, single and DKO mice at P2 and P7…… Page 2

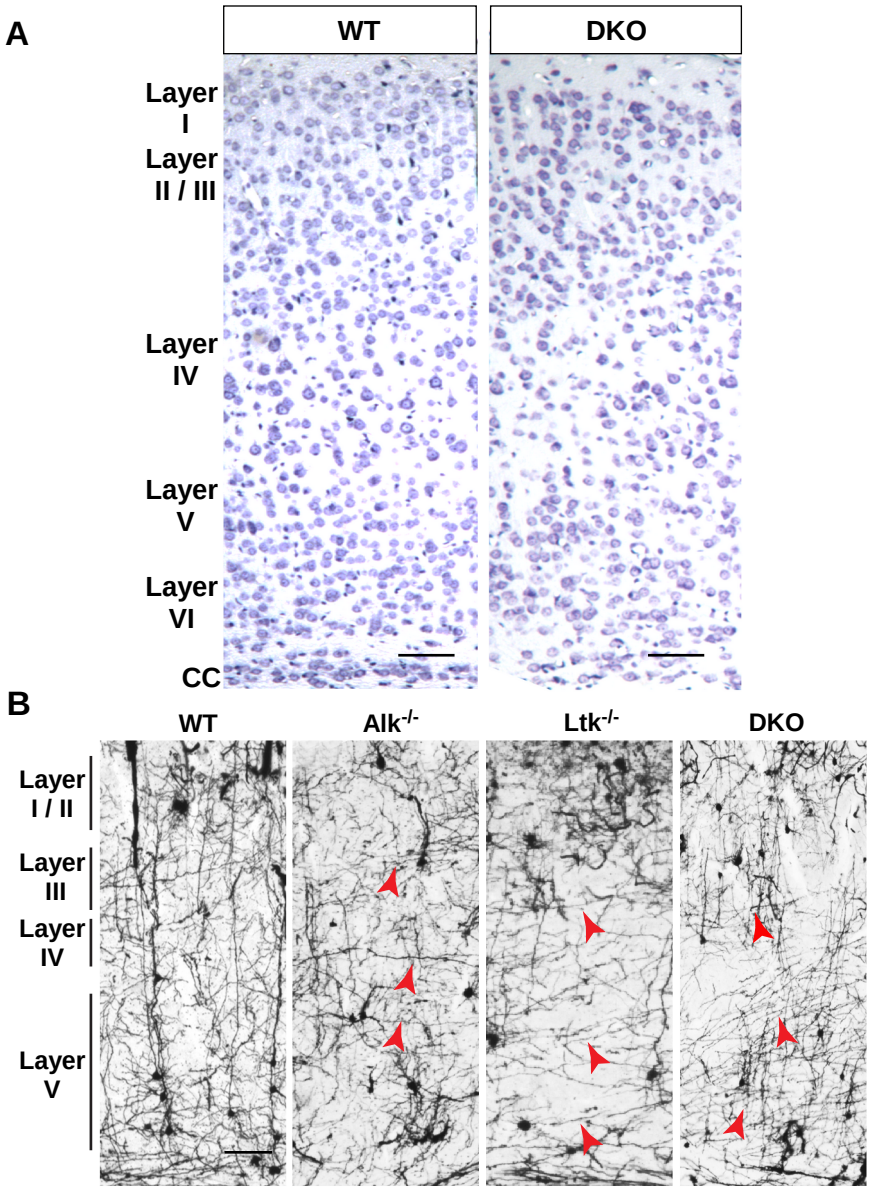
Appendix Figure S3: Change of expression or activity of Ltk and Alk results in defects in neuronal polarity…… Page 3-4

Appendix Figure S4: Performance of mice in light-dark box and in puzzle box tests…… Page 5-6

Appendix Table S1: Sequences of primers used for genotyping…… Page 7

Appendix Table S2: Antibody list…… Page 8

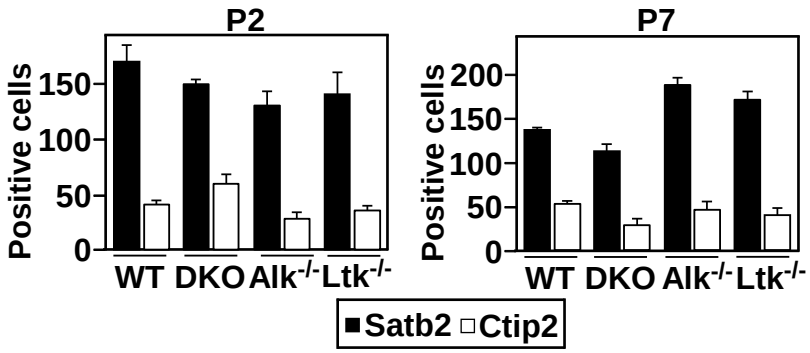
Appendix Table S3: Sequences of primers used for Real-time PCR …… Page 9



Appendix Figure S1. Analysis of Coronal sections of WT and Ltk/Alk knockout mice by Nissl and Golgi staining.

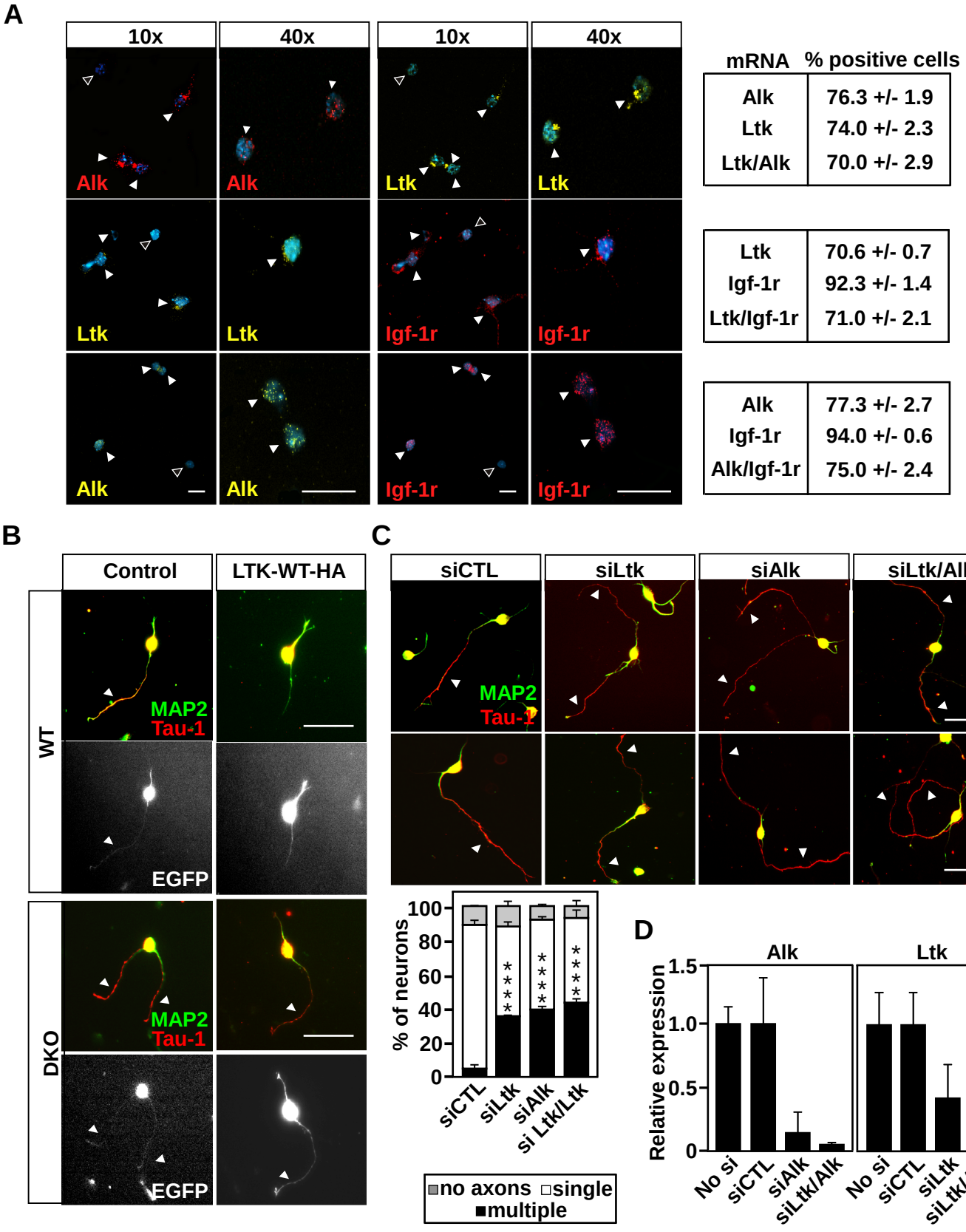
A Analysis of cortical layering *in vivo* by Nissl staining of adult WT and DKO murine brains. Nissl-stained coronal sections reveal a similar pattern of cortical layering in wild type (WT) and DKO adults. Scale bars are 100 µm.

B Golgi stains of adult cortices in wild-type (WT), single (Ltk$^{-/-}$and Alk$^{-/-}$) and double (DKO) knockout mice show defects in neuronal projections. Representative coronal sections obtained from an independent biological experiment from those in Fig. 3E are shown. Examples of aberrant projections in pyramidal neurons in knockout mice are marked (red arrowheads). Scale bars are 100 µm.



Appendix Figure S2. Ctip2 and Satb2 positive cells in WT, single and DKO mice at P2 and P7.
Quantitation of Ctip2 and Satb2 positive cells in all 8 bins within the cortex of WT, single and DKO mice at P2 and P7 in a total area corresponding to 100 µM x 600 µM.

Data information: Data are presented as the mean ± SEM of 3 independent experiments.


A
10x
40x
10x
40x
Alk
Ltk
Igf-1r
mRNA % positive cells
Alk 76.3 +/- 1.9
Ltk 74.0 +/- 2.3
Ltk/Alk 70.0 +/- 2.9
Ltk 70.6 +/- 0.7
Igf-1r 92.3 +/- 1.4
Ltk/Igf-1r 71.0 +/- 2.1
Alk 77.3 +/- 2.7
Igf-1r 94.0 +/- 0.6
Alk/Igf-1r 75.0 +/- 2.4
B
Control
LTK-WT-HA
WT
DKO
MAP2
Tau-1
EGFP
C
siCTL
siLtk
siAlk
siLtk/Alk
% of neurons
siCTL
siLtk
siAlk
si Ltk/Ltk
no axons
single
multiple
D
Alk
Ltk
Relative expression
No si
siCTL
siAlk
siLtk/Alk

Appendix Figure S3. Change of expression or activity of Ltk and Alk results in defects in neuronal polarity.

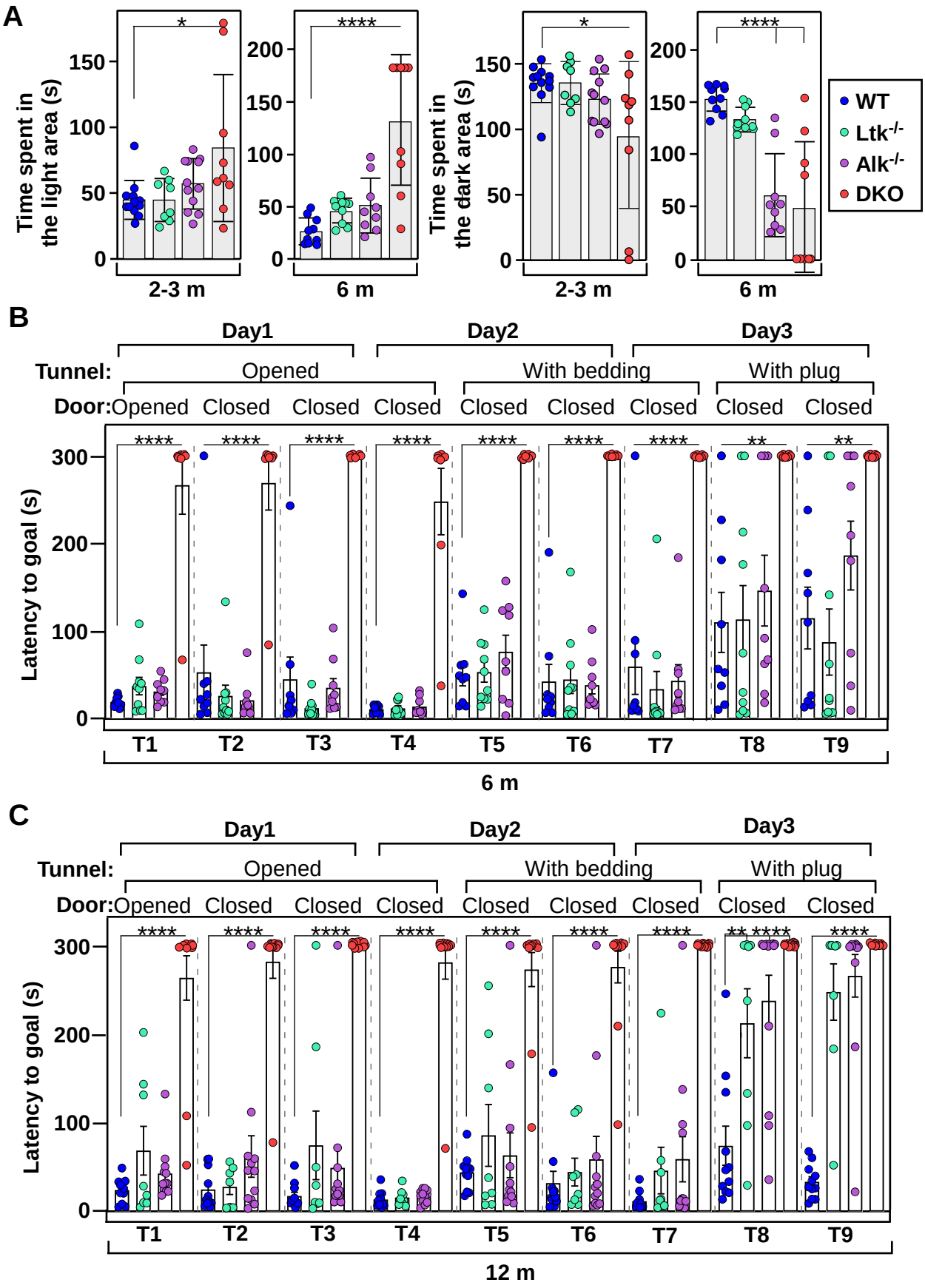
A Analysis of mRNA expression of Ltk, Alk and Igf-1r in isolated neurons. Expression of Alk, Ltk and Igf-1r in isolated primary cortical neurons from WT mice was determined by single molecule *in situ* analysis. Independent images taken at 10X and 40X magnification are shown. Filled arrowheads mark positive cells and open arrowheads mark negative cells. Scale bars are 200 μm. Quantitation of the percent of positive cells was tabulated (right).

B Additional representative images of dissociated WT and DKO cortical neurons, electroporated with plasmids encoding EGFP alone (control) or together with HA-tagged LTK-WT (as in Figure 3C) are shown. Cells were fixed 38 h after plating and then stained for Tau-1 (axons, red)) and MAP2 (dendrites, green) with transfected cells identified by EGFP staining (white). Scale bars are 20 μm.

C Abrogation of the expression of Ltk, Alk or both in cortical neurons using siRNAs results in defects similar to that observed in neurons isolated from knockout mice. WT cortical neurons were transfected with siCtl, siLtk and/or siAlk. Representative images of cells fixed at 38 h and stained with Tau-1 (axons, red) and MAP2 (dendrites, green) are shown. Scale bars are 20 μm.

D Knockdown efficiency in neurons was evaluated by real-time PCR.

Data information: Quantitation of the percent of positive cells in (A) was plotted from 3 independent biological experiments and a minimum of 50 cells per condition. Quantitation of percent of neurons with multiple, single or no axons in (C) is plotted as the mean ± SEM of n=150 neurons from 3 independent biological experiments. Data in (D) are plotted as mean ± SD from 3 independent biological experiments. Statistical significance: ****$p<0.0001$ by one-way ANOVA using Dunnett's test.


A
Time spent in the light area (s)
Time spent in the dark area (s)
2-3 m
6 m
WT
Ltk-/-
Alk-/-
DKO
B
Day1
Day2
Day3
Tunnel:
Opened
With bedding
With plug
Door:Opened Closed Closed Closed Closed Closed Closed Closed Closed
Latency to goal (s)
T1 T2 T3 T4 T5 T6 T7 T8 T9
6 m
C
Day1
Day2
Day3
Tunnel:
Opened
With bedding
With plug
Door:Opened Closed Closed Closed Closed Closed Closed Closed Closed
Latency to goal (s)
T1 T2 T3 T4 T5 T6 T7 T8 T9
12 m

Appendix Figure S4. Performance of mice in light-dark box and in puzzle box tests.

A Light-dark box. Time spent in the light or dark areas of individual mice of 2-3 or 6 months of age of the indicated genotypes is plotted.

B, C Puzzle-box test. Latency to reach the goal box during the 9 trials of the test is plotted for each individual 6 (B) or 12 (C) month old mouse of the indicated genotypes.

Data information: Results in all panels are plotted as mean ± SEM. Data were analyzed using one-way ANOVA and comparisons to WT were performed using Dunnett's test (****$p<0.0001$, **$p<0.01$, *$p<0.05$, ns, not significant, n=8-12 mice/group, n represents biological replicates).

Appendix Table S1: Sequences of primers used for genotyping

Gene	Forward	Reverse
Alk WT	ACC CCC TCA CAG CGG ACA CCT ATC	TGG GGA CAG GGG CAG ATG ATT GAC
Alk neo	ATC TCC TGT CAT CTC ACC TTG CTC	GTA AAG CAC GAG GAA GCG GTC AGC
Ltk WT	GCC AAC CTA CCG CAA GCC CTC TGA T	AAT AGT AAG GGT TGG GTG CTG TCC
Ltk neo	ATC TCC TGT CAT CTC ACC TTG CTC	GTA AAG CAC GAG GAA GCG GTC AGC

Appendix Table S2: Antibody list

Antibody	Host	Application	Dilution	Suppliers	Catalog number
MAP2	Mouse	ICC	1:400	Millipore	MAB3418
NeuN	Rabbit	IHC	1:500	Cell Signaling	12943
Tau-1 (PC1C6)	Mouse	ICC	1:200	Millipore	MAB3420
SOX2	Mouse	IHC	1:50	Santa Cruz	sc-365823
TBR2	Rabbit	IHC	1:200	Abcam	ab23345
SATB2	Rabbit	IHC	1:500	Abcam	ab51502
PAX6	Rabbit	IHC	1:100	Covance	PRB-278P
TUJ-1	Mouse	ICC	1:500	BioLegend	MMS-435P
BrDU	Rat	IHC	1:1000	Abcam	ab142567
CTIP2	Rat	IHC	1:300	Abcam	ab18465
ALK (D5F3)	Rabbit	WB	1:1000	Cell Signaling	3633
ALK (D5F3)	Rabbit	IP	1:100	Cell Signaling	3633
pALK (Tyr 1586)	Rabbit	WB	1:1000	Cell Signaling	3348
pAKT (Ser 473)	Rabbit	WB	1:1000	Cell Signaling	9271
AKT	Rabbit	WB	1:1000	Cell Signaling	9272
GSK3β (27C10)	Rabbit	WB	1:1000	Cell Signaling	9315
pGSK3β (Ser 9)	Rabbit	WB	1:1000	Cell Signaling	9323
IGF-1Rβ (D23H3)	Rabbit	WB	1:1000	Cell Signaling	9750
IGF-1Rβ (D23H3)	Rabbit	IP	1:100	Cell Signaling	9750
pIGF-1Rβ (Tyr 1135/1136)	Rabbit	WB	1:1000	Cell Signaling	3024
IGF-1Rα (24-60)	Mouse	NA	1.5 µg/µl	ThermoFisher	MA5-13817
Flag M2	Mouse	WB	1:3000	Sigma	F3165
Flag M2	Mouse	IP	1:1000	Sigma	F3165
HA	Rat	WB	1:1000	Roche	11867423001
GST	Rabbit	WB	1:1000	Cell Signaling	2625
GFP	Rabbit	WB	1:1000	Cell Signaling	2555
GFP	Mouse	IP	1:100	Santa Cruz	sc9996
GAPDH	Rabbit	WB	1:10000	Sigma	G9545

Appendix Table S3: Sequences of primers used for Real-Time PCR

Gene	Forward	Reverse
Ltk	CTC ATT CTG CTG GAG CTG ATG TCT	TGC AAT AGG TCC TGC ATG GTC AGA
Alk	CCC GAG TAT AAG CTG AGC AAG	TCA GGT CAC TGA TGG AGG AA
Gapdh	CAC ACC GAC CTT CAC CAT TTT	GAG ACA GCC GCA TCT TCT TGT
Igf-1r	CAG CAC TCG TTG TTC TCG GT	AGC CCA TGT GTG AGA AGA CC
Hprt1	TCA GTC AAC GGG GGA CAT A	GGG GCT GTA CTG CTT AAC CAG
Alkal2	TGA AAC ATC TCA CAG GTC CTC T	GAT GGT GCA GT TCT CGT GT